

A TRIASSIC, JURASSIC AND CRETACEOUS TIME SCALE

FELIX M. GRADSTEIN

Saga Petroleum a.s., Kjorboveien 16, Postboks 490, N-1301 Sandvika, Norway

FRITS P. AGTERBERG

Geological Survey of Canada, Ottawa, Ontario, K1A OE8, Canada

JAMES G. OGG

Department of Earth and Atmospheric Sciences, Purdue University, West Lafayette, IN 47907

JAN HARDENBOL

826 Plainwood Drive, Houston, TX 77079-4227

PAUL VAN VEEN

Norsk Hydro Research Centre, N-5020 Bergen, Norway

JACQUES THIERRY

6 Université de Bourgogne, Centre des Sciences de la Terre, 6 Bd. Gabriel, 2100 Dijon, France

AND

ZEHUI HUANG

Atlantic Geoscience Centre, P.O. Box 1006, Dartmouth, Nova Scotia, B2Y 4A2, Canada

ABSTRACT: We present an integrated geomagnetic polarity and stratigraphic time scale for the Triassic, Jurassic, and Cretaceous Periods of the Mesozoic Era, with age estimates and uncertainty limits for stage boundaries. The time scale uses a suite of 324 radiometric dates, including high-resolution $^{40}\text{Ar}/^{39}\text{Ar}$ age estimates. This framework involves the observed ties between (1) radiometric dates, biozones, and stage boundaries and (2) between biozones and magnetic reversals on the seafloor and in sediments. Detailed attention is given to chronostratigraphic calibration of stage boundaries using tetyan and boreal biozonations. Interpolation techniques to arrive at a geochronology include maximum likelihood estimation, smoothing cubic spline fitting, and magnetostratigraphy. The age estimates for the 31 stage boundaries (Ma with uncertainty in my to 2 standard deviations), and the duration of the preceding stages (in my) are:

Maastrichtian/Danian (Cretaceous/Cenozoic)	65.0 ± 0.1 Ma	6.3 my
Campanian/Maastrichtian	71.3 ± 0.5	12.2
Santonian/Campanian	83.5 ± 0.5	2.3
Coniacian/Santonian	85.8 ± 0.5	3.2
Turonian/Coniacian	89.0 ± 0.5	4.5
Cenomanian/Turonian	93.5 ± 0.2	5.4
Albian/Cenomanian	98.9 ± 0.6	13.3
Aptian/Albian	112.2 ± 1.1	8.8
Barremian/Aptian	121.0 ± 1.4	6.0
Hauterivian/Barremian	127.0 ± 1.6	5.0
Valanginian/Hauterivian	132.0 ± 1.9	5.0
Berriasian/Valanginian	137.0 ± 2.2	7.2
Tithonian/Berriasian (Jurassic/Cretaceous)	144.2 ± 2.6	6.5
Kimmeridgian/Tithonian	150.7 ± 3.0	3.4
Oxfordian/Kimmeridgian	154.1 ± 3.2	5.3
Callovian/Oxfordian	159.4 ± 3.6	5.0
Bathonian/Callovian	164.4 ± 3.8	4.8
Bajocian/Bathonian	169.2 ± 4.0	7.3
Aalenian/Bajocian	176.5 ± 4.0	3.6
Toarcian/Aalenian	180.1 ± 4.0	9.5
Pliensbachian/Toarcian	189.6 ± 4.0	5.7
Sinemurian/Pliensbachian	195.3 ± 3.9	6.6
Hettangian/Sinemurian	201.9 ± 3.9	3.8
Rhaetian/Hettangian (Triassic/Jurassic)	205.7 ± 4.0	3.9
Norian/Rhaetian	209.6 ± 4.1	11.1
Carnian/Norian	220.7 ± 4.4	6.7
Ladinian/Carnian	227.4 ± 4.5	6.9
Anisian/Ladinian	234.3 ± 4.6	7.4
Olenekian/Anisian	241.7 ± 4.7	3.1
Induan/Olenekian	244.8 ± 4.8	3.4
Tatarian/Induan (Permian/Triassic)	248.2 ± 4.8	

The uncertainty in the relative duration of each individual stage is much less than the uncertainties on the ages of the stage boundaries.

INTRODUCTION

The geological time scale for the Triassic, Jurassic, and Cretaceous Periods proposed in this study is composed of standard stratigraphic units (stages) calibrated in millions of years, with an uncertainty estimate at each level. Stratigraphically critical data underpinning this large framework of isotopic age dates

involve the observed ties between (1) radiometric dates, biozones, and stage boundaries and (2) biozones and magnetic reversals on the seafloor and in sediments.

The Cenozoic time scale is primarily calibrated from biosтратigraphic correlations to magnetic polarity chronos, which in turn are scaled according to magnetic anomaly profiles from the

South Atlantic pinned to a selected set of radiometric ages (e.g., Berggren and others, 1992; Cande and Kent, 1992; Berggren et al., this volume). In contrast, the Mesozoic time scale lacks a single unifying interpolation concept, because magnetic anomaly profiles only extend back to the Callovian stage, and much of the middle Cretaceous Period lacks a magnetic anomaly signature. In addition, the radiometric database has inadequate precision to constrain the age assignment of most stage boundaries. Therefore, whereas portions of the Mesozoic time scale can be exactly determined by a combination of radiometric ages on biostratigraphically controlled sections, the majority of the stage boundaries have been assigned through geological and mathematical interpolation methods.

Differences in selection criteria for radiometric ages and variations in interpolation methods have led to a bewildering array of Mesozoic time scales within the past two decades (Figs. 1–3).

It is possible to calculate a Mesozoic time scale with estimates of uncertainty for the age of each stage boundary. The derivation of such a numerical scale depends on sufficient and stratigraphically meaningful ages from isotopic measurements in magmatic intrusions, bentonites, glauconites and other rocks. In this regard, there have been approximately 65 well-calibrated Mesozoic age dates published since the previous array of time

scales (e.g., Odin, 1982; Snelling, 1985; Kent and Gradstein, 1985, 1986; Haq and others, 1988; Harland and others, 1990). Also, improvements in calibrations of stages and standard zones and development of better interpolation techniques allow significant updates to previously proposed age estimates for the stage boundaries in the Triassic, Jurassic, and Cretaceous Periods.

Frequently cited geologic time scale studies are abbreviated as follows: Harland and others (1982) is PTS82; Odin (1982) is NDS82; Kent and Gradstein (1985) is KG85, also referred to as part of the Decade of North America Geology (DNAG) scale (Palmer, 1983); Haq and others (1988) is EX88; Harland and others (1990) is PTS89; Cande and Kent (1992) is CK92; and Obradovich (1993) is OB93.

In this study we present the data and methods selected to arrive at the age estimates for the 31 Mesozoic stage boundaries. All age dates and stage boundary estimates are accompanied by two standard deviation ($\pm 2\sigma$) error bars. Portions of the methodology and the Mesozoic time scale were reported earlier (Gradstein and others, 1994), and the numerical ages for the standard stages are incorporated in a series of Mesozoic-Cenozoic chronostratigraphic charts (Hardenbol and others, *in de* Graciansky and others, Mesozoic-Cenozoic Sequence Stratigraphy of European Basins, SEPM Special Publication, in prep.).

Comparison of Cretaceous Time Scales

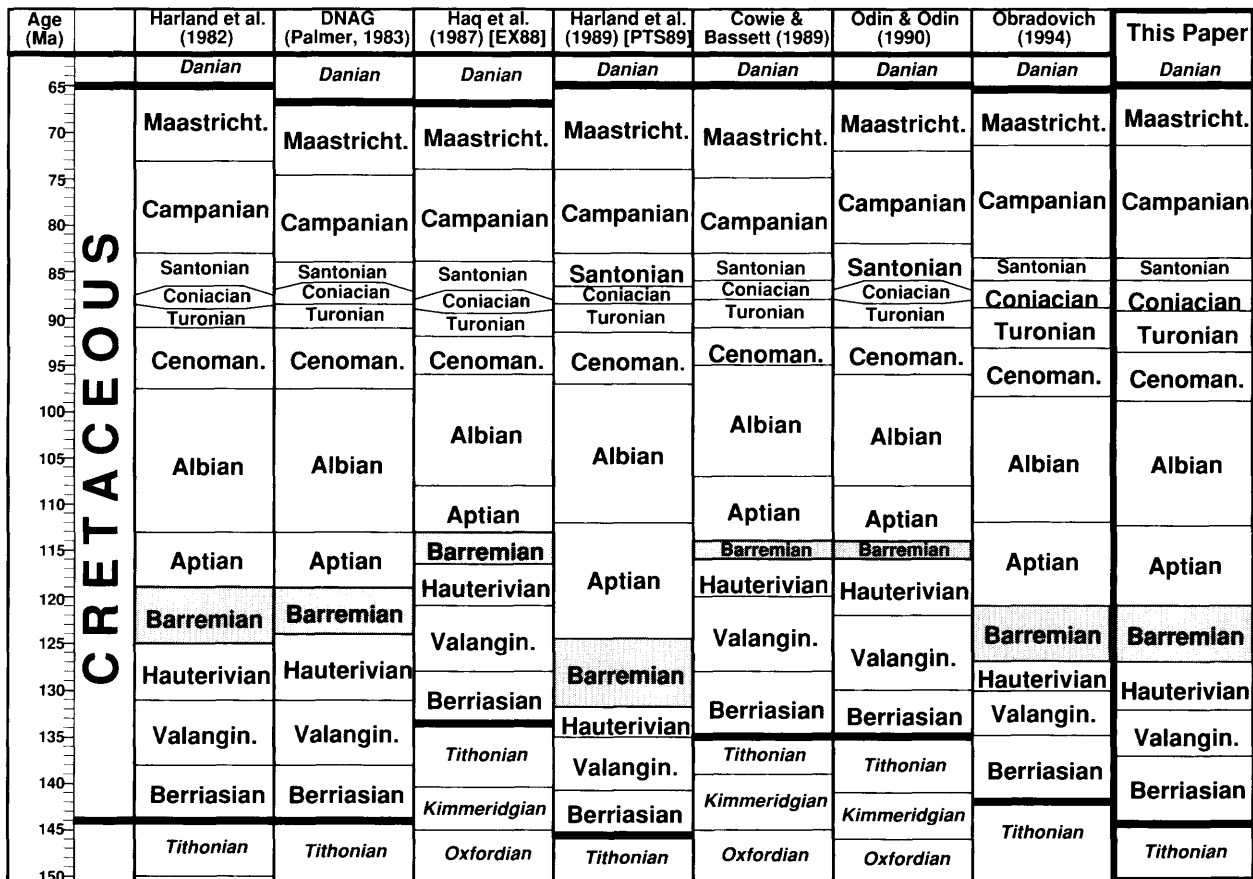


FIG. 1.—Comparison of Cretaceous time scales.

Comparison of Jurassic Time Scales

Age (Ma)	Harland et al. (1982)	DNAG (Palmer, 1983)	Haq et al. (1987) [EX88]	Harland et al. (1989) [PTS89]	Cowie & Bassett (1989)	Odin & Odin (1990)	This Paper
130	Hauterivian	Hauterivian		Barremian		Valanginian	Hauterivian
135	Valanginian	Valanginian	Berriasian	Hauterivian	Berriasian	Berriasian	Valanginian
140	Berriasian	Berriasian	Tithonian	Valanginian	Tithonian	Tithonian	Berriasian
145	Tithonian	Tithonian	Kimmeridg.	Berriasian	Kimmeridg.	Kimmeridg.	
150	Kimmeridg.	Kimmeridg.	Oxfordian	Tithonian	Oxfordian	Oxfordian	Tithonian
155	Oxfordian	Oxfordian	Callovian	Kimmeridg.	Callovian	Callovian	Kimmeridg.
160	Callovian	Callovian	Bathonian	Oxfordian	Bathonian	Bathonian	Callovian
165	Bathonian	Bathonian	Bajocian	Callovian	Bathonian	Bathonian	Bathonian
170	Bajocian	Bajocian	Aalenian	Bajocian	Bajocian	Bajocian	Bajocian
175	Aalenian	Aalenian	Toarcian	Aalenian	Toarcian	Toarcian	Aalenian
180	Toarcian	Toarcian	Pliensbach.	Toarcian	Pliensbach.	Pliensbach.	Toarcian
185	Pliensbach.	Pliensbach.	Sinemurian	Pliensbach.	Sinemurian	Sinemurian	Pliensbach.
190	Sinemurian	Sinemurian	Hettangian	Sinemurian	Hettangian	Hettangian	Sinemurian
195	Hettangian		Rhaetian		Rhaetian		Rhaetian
205		Norian	Rhaetian	Norian	Norian	Norian	Norian
210							
215	Rhaetian						

FIG. 2.—Comparison of Jurassic time scales.

PREVIOUS MESOZOIC TIME SCALES

During the last two decades, the Mesozoic geologic time scale has undergone various improvements. The stratigraphic calibration of the Hawaiian lineation spreading profile (Larson and Hilde, 1975) was adapted for scaling of geologic stages by Larson and Hilde (1975), DNAG, and OB93. Databases of radiometric ages have been statistically analyzed with various best-fit methods to estimate ages of stage boundaries (PTS82 and PTS89). Comparisons in duration of stages and age of stage boundaries for selected Mesozoic geologic time scales are documented in Figures 1, 2 and 3.

Among widely used scales, PTS89 stands out because of its authoritative radiometric database, developed and expanded since Armstrong (1978) and PTS82, its elegant use of the chronogram method for unbiased age interpolation, and its efforts to provide biochronologic underpinning. Unfortunately, no error bars on stage boundary age estimates were calculated, but its balanced approach in dealing with glauconite versus high-temperature age dates has provided a measure of stability for age estimates on Early Cretaceous and Jurassic stage boundaries. PTS89 takes glauconite-based age estimates as minimum ages for the age calibration of Mesozoic stratigraphic boundaries older than 115 Ma. Indeed, many Jurassic-Cretaceous glauco-

nite ages are significantly younger than their high-temperature counterparts (e.g., Gradstein and others, 1988). PTS89 relied heavily on chronograms (see below) and smoothing of its results in a plot of chrons versus ages, where chrons are a substitute for biozones per stage unit. For example, the Jurassic/Cretaceous boundary is between 13 and 17 my older using high-temperature minerals rather than glauconite dates (PTS89, and Table 1).

If we take a brief look at changes in method philosophy among the three key scales available to date for the whole Mesozoic Era (i.e., PTS89, Odin and Odin, 1990, and EX88), we see a greater reliance on direct linkage of low- and high-temperature radiometric dates with stratigraphic levels by Odin and Odin (1990) and more reliance on interpolation methods with the other two scales. Ideally, precise dating at distinct stratigraphic boundaries is preferred; however, such precision is scarce below the Upper Cretaceous Period. EX88 largely used glauconites, which explains why the Jurassic/Cretaceous boundary in EX88 is at 131 Ma and in PTS89 at 145 Ma. EX88 employed a composite of several spreading profiles in different oceans to scale the Late Jurassic through Early Cretaceous time scales and also used the zones versus ages plots for further smoothing of results. It is not clear if the composite spreading profile in fact increases reliability of the interpolation.

Comparison of Triassic Time Scales

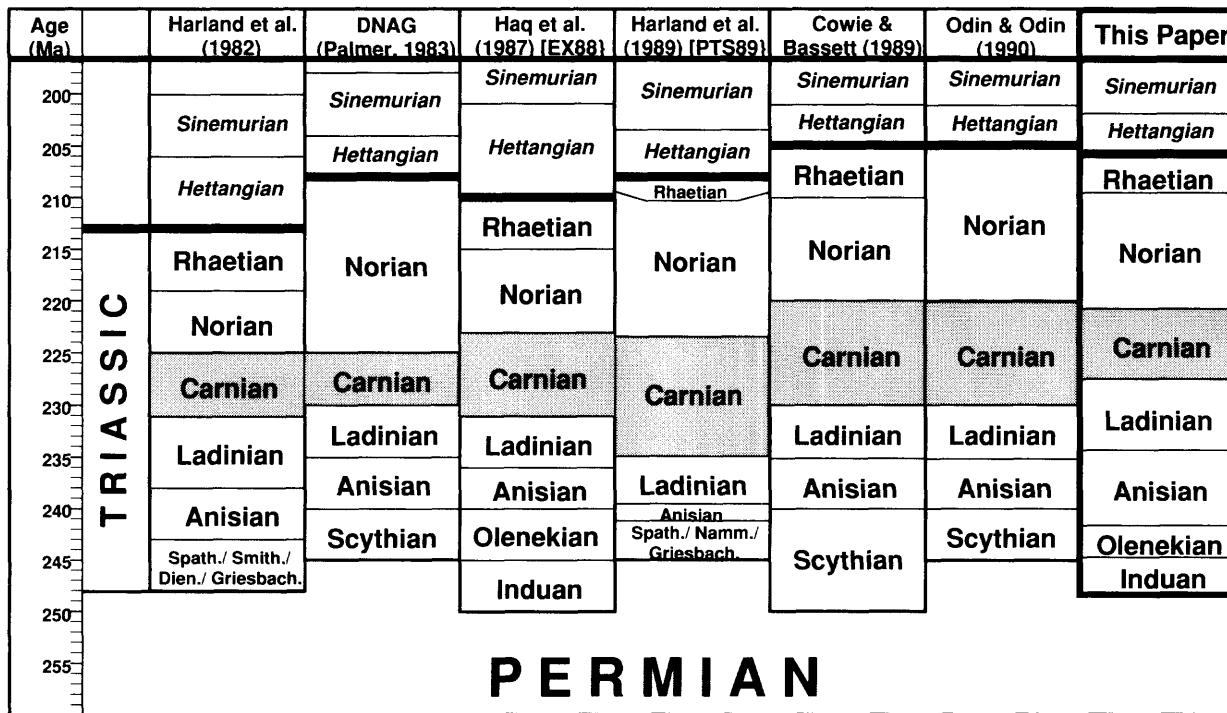


FIG. 3.—Comparison of Triassic time scales.

EX88, KG85, NDS82, and van Hinte (1976) relied on biochronology to interpolate the duration of Jurassic stages. The theory assumes that the numerous, short-lived ammonite zones for the Jurassic Period have approximately equal duration, the result of regular evolutionary change. Assuming age tiepoints at the top and bottom of Jurassic Period, the average duration of each zone is estimated (approximately 1 my). From the number of zones per stage, the duration of that stage was estimated. KG85 also took into account some intra-Jurassic control points. The method is not necessarily accurate, but it is detailed, because the number of standard ammonite zones is relatively large. To minimize taxonomic bias, Westermann (1988) compiled independent sets of Jurassic zones and subzones from the different faunal provinces. Subzones were calibrated as 75% of the undivided length of zonal units and on average lasted 0.45 my.

The advent of $^{40}\text{Ar}/^{39}\text{Ar}$ radiometric dates for a significant part of the U.S. Western Interior Cretaceous (OB93), coupled to a detailed ammonite biostratigraphy (Cobban and others, 1994), is another significant improvement of late Mesozoic geochronology.

A Global Stratigraphic Chart was compiled under the auspices of the International Union of Geological Sciences (IUGS) by Cowie and Bassett (1989) incorporating scales from the stratigraphic working groups of IUGS. The chart reflects much of current stratigraphic usage. The Bureau de Recherches Géologiques et Minières and the Société Géologique de France published a stratigraphic scale and time scale compiled by Odin

and Odin (1990). Of the more than 110 defined boundaries, 20 lack radiometric data.

A major difference among time scales, for example, is the duration of the Aalenian Stage, using either KG85, EX88 or PTS89. Admittedly, there is a paucity of reliable radiometric dates in the middle Jurassic (Appendices 1, 2), but Jurassic standard ammonite zonations (e.g., Westermann, 1984, 1988; PTS89) indicate that the adjacent Toarcian and Bajocian Stages have double the number of ammonite subzones over the Aalenian, which casts doubt on the (unusually) long Aalenian Stage in EX88. As pointed out by Westermann (1984, 1988), the relative brevity of the Aalenian Stage in Europe has caused many debates. Despite the fact that the uncertainties on the ages of the Aalenian Stage boundaries exceed the estimate of the stage duration (see below), we predict with confidence that the Aalenian Stage is significantly shorter than the underlying Toarcian and the overlying Bajocian stage.

DATA AND STEPS IN TIME SCALE ANALYSIS

As explained earlier, no single unifying concept is available for Mesozoic time scale analysis and interpolation. In order to achieve a measure of objectivity and standardization, we combined several geological and statistical methods, while trying to assess and preserve estimates of analytical and stratigraphic uncertainty in the data. Statistics played a more major role for the parts of the Mesozoic time scale where age control is limited.

TABLE 1.—COMPARISON OF MAXIMUM LIKELIHOOD ESTIMATES

Stage	Parabola Peak Estimates ^a	Local Maximum Obtained by Scoring Method			
		High-Temperature Dates	Low-Temperature Dates	Combined High and Low Temperature	Probability ^b
Maa	66.06 (0.41)	65.98 (0.69)	66.18 (0.51)	6.11 (0.40)	0.145
Cam	71.58 (0.42)	71.99 (1.38)	71.96 (0.63)	71.96 (0.58)	0.508
San	82.54 (0.21)	82.32 (1.08)	83.12 (1.30)	82.61 (0.92)	0.320
Con	86.04 (0.26)	86.51 (0.59)	85.02 (0.73)	85.40 (0.58)	0.940
Tur	89.11 (0.27)	89.33 (1.26)	87.73 (0.44)	88.31 (0.28)	0.884
Cen	93.26 (0.20)	93.40 (0.16)	90.24 (0.41)	92.73 (0.18)	1.000
Alb	100.48 (0.34)	98.94 (0.30) ^c	96.62 (0.46)	98.41 (0.15)	0.992
Apt	108.33 (0.69)	112.18 (0.87) ^c	109.43 (0.62)	110.15 (0.41)	0.995
Bar	120.26 (0.74) ^c	121.43 (20.48) ^c	118.52 (0.98)	118.53 (0.95)	0.991
Hau	124.96 (0.53)	127.11 (0.88) ^c	118.52 (0.97)	125.01 (1.39)	1.000
Val	133.90 (0.93)	135.07 (2.59)	126.05 (1.64)	128.71 (1.59)	0.998
Ber	133.73 (0.95)	136.43 (0.96) ^c	129.40 (1.87)	132.37 (1.16)	1.000
Tit	147.75 (3.66)	148.77 (3.10)	130.75 (1.60)	136.36 (0.38)	1.000
Kim	145.72 (1.71)	149.81 (3.83)	139.32 (0.97)	139.99 (0.89)	0.996
Oxf	156.83 (0.69)	155.09 (1.80) ^c	147.26 (1.31)	153.42 (0.25)	1.000
Cal	161.85 (1.01)	159.05 (2.32) ^c	no solution	159.28 (2.25)	
Bat	163.27 (2.07)	164.28 (2.60) ^c	no solution	164.32 (2.56)	
Baj	165.22 (1.90)	166.31 (2.37) ^c	no solution	166.32 (2.40)	
Aal	178.10 (2.69)	177.32 (4.26)	no solution	178.18 (3.64)	
Toa	177.96 (2.81)	177.32 (4.10)	no solution	178.63 (3.38)	
Pli	181.05 (6.61)	180.15 (10.89)	187.82 (20.47)	182.24 (7.57)	0.370
Sin	196.30 (1.01)	196.47 (2.23) ^c	no solution	196.35 (2.29)	
Het	197.92 (0.70)	200.57 (0.67) ^c	no solution	200.55 (0.67)	
Rha	209.06 (1.65)	208.66 (3.32) ^c	no solution	208.69 (3.16)	
Nor	211.49 (2.61)	209.76 (4.06) ^c	no solution	210.76 (3.74)	
Car	223.67 (3.02)	223.44 (6.13) ^c	no solution	223.48 (5.68)	
Lad	233.89 (2.22)	233.69 (2.61) ^c	no solution	233.69 (2.59)	
Ani	236.55 (1.73)	236.51 (1.96) ^c	239.51 (8.63)	236.77 (1.77)	0.367
Ole	242.38 (2.81)	242.27 (3.54) ^c	239.51 (9.05)	241.99 (3.32)	0.612
Tat	243.63 (2.22)	244.75 (4.06) ^c	no solution	244.75 (4.06)	

Standard deviations in parentheses. For top of Barremian, standard deviation selected is parabola peak estimate instead of scoring result because of exceptionally flat local maximum.

^aBased on wider-range, high-temperature dates.

^bProbability that low-temperature estimate for low-temperature dates is younger than the high-temperature estimate of local maximum obtained by scoring method high-temperature dates.

^cResults used in Table 2.

The first step to build the Mesozoic time scale was to assess the age of key stratigraphic boundaries. Next, a database was built of selected radiometric estimates throughout the Mesozoic that are stratigraphically closely bracketed, analytically standardized and reasonably documented (Figs. 4, 5; Appendix 1). The majority of items were taken from the detailed list in PTS89 (their Table 4.2) that screened dates on excessive analytical uncertainty and anomalous stratigraphic position. The selection of Mesozoic dates in Appendix B of EX88, which form the basis of that time scale, was also reassessed, and the weighted means and standard errors recalculated (Appendix 1). Over 65 new and stratigraphically significant Triassic, Jurassic, and Cretaceous dates published since PTS89 and EX88 were added to the data file. The $^{40}\text{Ar}/^{39}\text{Ar}$ ages were recomputed to be in accordance with a 520.4 Ma age for the MMhb-1 laboratory standard.

The time scale proposed in this study uses only high-temperature radiometric age assignments. Low-temperature dates are significantly younger for a number of stage boundaries where there are many low- and high-temperature dates (Table 1); this is a good reason for not using low-temperature dates, of which there are few in pre-Callovian rocks (Fig. 5).

Next, we interpolated the Maastrichtian through Cenomanian analytical data from OB93, in combination with the new esti-

Distribution of Radiometric Dates

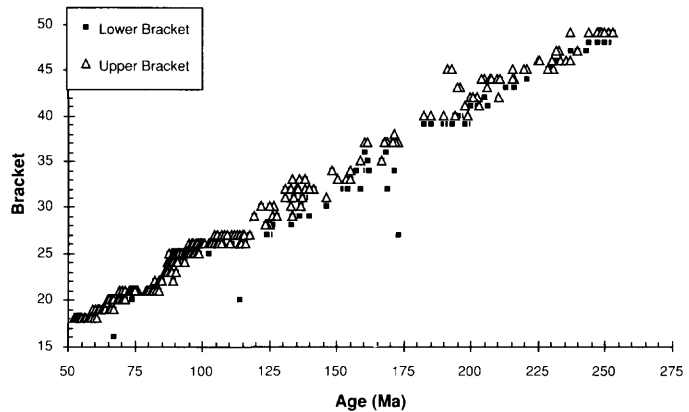


FIG. 4.—Distribution of radiometric dates. The bracket refers to the relative age of sediments immediately above and below the dated level.

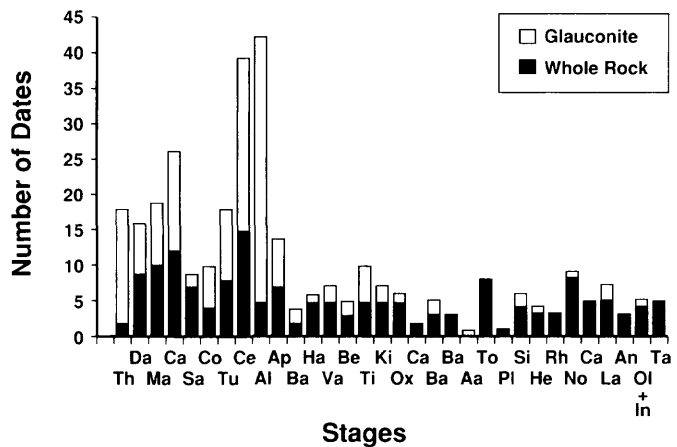


FIG. 5.—Radiometric dates by type and by stage.

mate for the K/T boundary to arrive at dates with narrow uncertainty limits for the Late Cretaceous stage boundaries. Aptian and Albian boundary ages were calculated with maximum likelihood estimation. The Barremian through Oxfordian interval was age calibrated with the Hawaiian seafloor spreading profile and then averaged with the best estimates from maximum likelihood age estimation. The ages of pre-Oxfordian Stage boundaries come from maximum likelihood estimation; poor estimates for the Pliensbachian and Anisian/Ladinian Stage boundaries were constrained with single, well-calibrated direct age estimates from the literature.

The resulting age estimates for Triassic and Early-Middle Jurassic stage boundaries were smoothed with a spline to achieve statistical improvements for age estimates of stage boundaries with larger uncertainty. This spline scaling incorporated a suite of detailed ammonite zonations for the Tethyan and Boreal faunal realms.

Each difference between ages of two successive stage boundaries provides an estimate of the duration of the enclosed stage. It is inversely proportional to average sedimentation rate for this

stage. The uncertainty in relative duration of each individual stage is much less than the uncertainties on the ages of the stage boundaries. It is not possible to estimate standard deviations for the durations because of lack of information on serial correlation of the stage boundary age estimates. As shown in the last column of Table 1, the ratio of stage duration estimates for this Mesozoic time scale and PTS89 fluctuates between 0.2 and 1.7. Our duration estimates are relatively precise. Nevertheless, the large differences between results based on successive time scales suggest that the Mesozoic time scale needs further improvement, especially if it is to be used for basin modelling involving sedimentation rates.

Three statistical methods were used repeatedly during the construction of the Mesozoic time scale: (1) maximum likelihood estimation to combine stratigraphic with geochronological uncertainty for individual stage boundaries; (2) averaging of statistically independent estimates for the same stage boundary; and (3) spline-curve fitting for adjustment of individual stage boundary estimates using variable precision estimates for adjacent stages. These procedures will be discussed in the following sections.

AGE ESTIMATES FOR SELECTED STRATIGRAPHIC BOUNDARIES

Below, we outline differing age assignments for key Mesozoic stratigraphic boundaries and their age estimates entered in calculation of the Mesozoic time scale.

Permian/Triassic Boundary

Estimates for the age of the Permian/Triassic boundary vary between 248 Ma in EX88 and 245 Ma in PTS89. As pointed out by these authors, the available data were such that the age could be placed in a window between 255/260 and 240 Ma. Recently, new evidence has become available to better constrain the age of this boundary between Paleozoic and Mesozoic strata.

Claoue-Long and others (1991) used ion microprobe dating of zircons on a bentonite in the Chinese stratotype section through the Permian-Triassic boundary (Item 319 in Appendix 1). The bentonite is 5 cm thick and occurs at the boundary, between the uppermost Permian Changxing Formation and the overlying Mixed Fauna Bed 1 of the Chinglung Formation with (?) *Otoceras* ammonites, and below the Mixed Fauna Bed 2 with *Hindeodus parvus* conodonts of definite earliest Triassic age. The Pb/Th/U radiometric age for the boundary bed is 251.2 ± 3.4 Ma (2σ). Since the *Otoceras* identifications are uncertain, the age may be a maximum one for the boundary (E. T. Tozer, as cited by Claoue-Long and others (1991)). The mixed fauna beds indicate slight reworking, which may also pertain to the zircon in the bentonite. Nakazawa (1992) suggests a latest Permian age for the boundary clay; on the basis of the occurrence of Permian conodonts, Yin (1993) supports a latest Permian age of this horizon at the Meishan locality. Hence, the boundary bed may actually be slightly older than the Permian/Triassic boundary in less condensed sections.

New data have become available using sanidine from the same rock sample in the bentonite bed (Zhang Zichao, as cited by Odin, 1992b; Item 320 in Appendix 1). Ar/Ar dates average at 255.9 ± 5.6 Ma (2σ). The Rb/Sr isochron age on the same

sanidine is 250 ± 6 Ma (2σ). The Ar/Ar date uses a standard different from MMhb-1 at 520.4 Ma.

Further radiometric evidence for the age of the Permian/Triassic boundary comes from Ar/Ar and K/Ar dates on flood basalts in Siberia at the Permian-Triassic boundary (Renne and Basu, 1991). Detailed sampling and analysis resolve that virtually all flood basalt erupted between 248.3 ± 0.3 and 247.5 ± 0.7 Ma (Items 317 and 318 in Appendix 1). Following Nalivkin (1973), the Siberian traps straddle the Permian/Triassic boundary with Tatarian ostracod clays interbedded in its lower tuffaceous part and Early Triassic Estheria molluscs in shales of the upper tuffs.

If we consider the Chinese dates to be maximum ones, which overlap at the 95% confidence level with the Siberian flood basalt dates (which admittedly are biostratigraphically less well constrained), a 248 Ma age for the Permian/Triassic boundary is reasonable. This age is a best estimate for the onset of the major volcanic activity that may have associated the major chemical and biotic changes that separate the Paleozoic from the Mesozoic Era (e.g., Holser and Magaritz, 1987; Holser and others, 1991).

Ladinian/Anisian Boundary

An important anchor point in the Triassic Period is dating of the Ladinian/Anisian boundary in the Grenzbitumen horizon in Switzerland (Hellmann and Lippolt, 1981; Forster and Warrington, 1985). Both K/Ar and Ar/Ar dates on alkali feldspars were done from tuff layers in the basal part of the lowermost Ladinian *Nevadites* (tethyan) ammonite Zone (Brack and Rieber, 1993). The best dates are derived from homogenous and clear, high-sanidine feldspars (type G), which average at 232 ± 9 Ma (2σ) for K/Ar and 233 ± 7 Ma (2σ) for Ar/Ar, from which Hellmann and Lippolt (1981) estimate the boundary to be 232 ± 9 Ma (2σ) (Items 309 and 310 in Appendix 1). Odin (1982) suggests 232.7 ± 4.5 Ma (2σ) for K/Ar and 232 Ma plateau age for Ar/Ar in the waterclear sanidine feldspars (NDS196).

Triassic/Jurassic Boundary

The current working definition of the Triassic/Jurassic boundary is the migration influx of the ammonite *Planorbis* observed in the Blue Lias of the United Kingdom. Age estimates for the Triassic/Jurassic boundary range from 205 Ma to 213 Ma (Fig. 3).

EX88 quote an age of 206.0 ± 12.0 Ma for the Hettangian/Sinemurian boundary, using data referred to NDS82 listing 202. NDS82 quote 190–200 Ma as a most likely age bracket for these dates from the West Rock and Mt. Carmel sills, Hartford Basin, eastern United States. PTS89 uses an age of 198.50 ± 5.78 Ma referred to the Hettangian-Sinemurian Stages, for the same item NDS202. Forster and Warrington (1985) give a detailed account of all the dates and errors and use 196 ± 4.5 Ma for the Palisades Sills and 195 ± 4.2 Ma for the Mt. Carmel sills (in agreement with NDS202, p. 878). The relative age using palynofloral evidence, is quoted as early Liassic, which unfortunately is broad. We follow Forster and Warrington's (1985) use of the data and assign the 195 and 196 Ma estimates (Appendix 1, items 278 and 279) an Hettangian-Sinemurian age.

The 196 Ma age for Hettangian-Sinemurian strata above the Triassic/Jurassic boundary agrees with the average U/Pb age of 194.12 ± 0.62 Ma (1σ) on zircons in the Cold Fish volcanics, British Columbia (Thorkelson and others, 1991, 1994; J. Mortensen, pers. commun., 1993; item 276, Appendix 1). Ammonites in sedimentary beds alternating with the volcanics include *Miltoceras* sp., *Tropidoceras* sp., *Metaderoceras* sp. aff. *talkeetnaense*, *Acanthopleuroceras* sp. aff. *A. stahli*, and *Metaderoceras evolutum* and assign the Cold Fish volcanics an early to middle Carixian (Early Pliensbachian) age (Thomson and Smith, 1992).

The post Triassic/Jurassic boundary ages of 196 and 194 Ma are consistent with 201–202 Ma as an approximate estimate for the Triassic/Jurassic boundary in eastern North America. The latter estimate derives from U/Pb zircon dating of the North Mountain basalt, Fundy Basin at 202 ± 1 Ma (1σ) and U/Pb and Ar/Ar ages of 201 ± 1 Ma (1σ) for correlative intrusives in the Newark Basin (Hodych and Dunning, 1992; Fowell and Olsen, 1993; Appendix 1, items 285 and 286).

However, interpretation of paleontologic criteria for correlation above and below the Triassic/Jurassic boundary to the basalt levels is far from straightforward. Post-Sinemurian *Calloaspisporites* is recorded above the lower basalts. Palynological assemblages at 30 m below the Jacksonwald Basalt in the Exeter Village section (Newark basin) contain predominantly vesiculate pollen (*Vallasporites ignacii*, *Patinasporites densus*, *Enzonaspisporites* spp.), referred to as latest Triassic age (Cornet and Olsen, 1985, Fowell and Olsen, 1993). The criterium for the Triassic/Jurassic boundary in the Newark basins is the preponderance of the pollen *Corollina meyeriana*, occurring 10 m below the lower Newark Basin basalts (Fowell and Olsen, 1993). Palynofloras in the basal Liassic Planorbis beds in southern England are also dominated by *Corollina* (e.g., Orbell, 1983). On the basis of Milankovitch cyclicity criteria, Fowell and Olsen (1993) suggest (a) that the disappearance of vesiculate pollen predates the *Corollina meyeriana* dominated assemblages by a maximum of 21,000 years, and (b) that the palynological placement of the Triassic/Jurassic boundary predates the Jacksonwald Basalt by an additional 21,000 years. Yet, in Alpine Europe and in contemporaneous sections in Western Europe, vesiculate pollen (e.g., *Vallasporites ignacii*, *Enzonaspisporites* sp. div.) disappear at the base of the *suessi* ammonoid zone (Warrington, 1974; Mostler and others, 1978; Morbey, 1978; Schuurman, 1979), probably below the base of the Rhaetian, approximately 3–4 my before the Triassic/Jurassic boundary. This suggests that Milankovitch cyclicity may not be applicable to approximate the time span between the disappearance of vesiculate pollen, the palynologically assigned Triassic/Jurassic boundary and the onset of basalt deposition in the Newark Basin.

The 201–202 Ma dates from the lower basalts of the Newark basins are assigned a Hettangian age (Items 285 and 286 in Appendix 1).

Oxfordian/Kimmeridgian Boundary

Dates near the Oxfordian/Kimmeridgian boundary anchor the beginning of the Hawaiian sequence of marine magnetic anomalies in magnetochronology.

U/Pb dating of zircons from igneous rocks pre- and post-Galice Formation (see discussion in Harper, 1984) of northern

California and southwestern Oregon bracket the *Buchia concentrica* mollusc Assemblage between 150.5 ± 2.0 and 157 ± 2.0 Ma, mid-middle Oxfordian to mid-late Kimmeridgian age (Appendix 1, items 244 and 253). This also constrains the Oxfordian/Kimmeridgian boundary to fall somewhere in this age bracket, with an average estimate near 154 Ma.

Pessagno and Blome (1990) combined new radiolaria and ammonite data in the lower level of the (basal) Galice Formation, Oregon, USA with *Buchia concentrica*, *Dichotosphinctes*, and *Miritusus*. This assemblage is assigned to the mid-Middle Oxfordian and only slightly younger than a level in the uppermost Rogue Formation with dacitic tuff breccia dated with U/Pb on zircons as 157.00 ± 2.00 Ma (Saleeby, 1984; item 253 in Appendix 1). By extrapolation, assuming a duration of 3 my for the younger Oxfordian, the Oxfordian/Kimmeridgian boundary is estimated to be 154 Ma.

Magnetic polarity chron M25 is at the Oxfordian/Kimmeridgian boundary in ammonite-zoned sections in Spain (Ogg and others, 1984). Ocean crust of marine magnetic anomaly M26r (Late Oxfordian) at Ocean Drilling Program Site 765, Argo Abyssal Plain, has an Ar/Ar age of 155.3 ± 3.4 Ma (Ludden, 1992; Item 251 in Appendix 1).

Jurassic/Cretaceous Boundary and Berriasian/Valanginian Boundary

The Tithonian/Berriasian Stage boundary or Jurassic/Cretaceous boundary does not have an internationally accepted definition, although several possible biostratigraphic markers have been correlated to magnetostratigraphy (Ogg and others, 1991a). A placement of the Jurassic/Cretaceous boundary at the top of the *Berriasella jacobi* ammonite Zone corresponds approximately to the base of magnetic polarity chron M18r (Ogg and Lowrie, 1986).

An alternate placement of the Jurassic/Cretaceous boundary at the base of this *B. jacobi* Zone (top of *Durangites* ammonite Zone) is used in our compilation in accordance with recent proposed boundary definitions (J. Remane, pers. commun., 1993).

Previous time scales have generally not specified the definition of the Jurassic/Cretaceous boundary and have proposed boundary ages ranging from 133 Ma to 146 Ma (Fig. 2). A contributing factor is the younger definition of the Jurassic/Cretaceous boundary used within the Boreal realm. The top of the regional Portland Stage of “uppermost Jurassic” strata is approximately equivalent to the top of the regional Volgian Stage, and these levels correlate approximately to the middle of the Berriasian Stage of the Tethyan realm (Mesezhnikov, 1988; Ogg and others, 1991a; Ph. Hoedemaeker, pers. commun., 1994). These regional Boreal stages are terminated by a significant unconformity, and the base of the overlying regional Ryazanian Stage of “lowest Cretaceous” may locally be equivalent to the upper Berriasian in the Tethyan realm.

The age of the Berriasian Stage is partially constrained by a U/Pb date of 137.1 ± 0.6 Ma from volcanic horizons in the Grindstone Creek section in northern California (Bralower and others, 1990; Appendix 1, item 232). Bralower and others (1990) assigned this level to late Middle Berriasian Age according to nannofossil assemblage ranges, correlated the level to polarity chron M16 and projected the age of the Jurassic/

Cretaceous boundary to be 141 Ma. This radiometric date and assigned stratigraphic age was a key control in the Early Cretaceous portion of the OB93 time scale (Obradovich, 1993; Fig. 1). However, the age assignment from the mollusc and nannofossil assemblages may be less precise than published (Ph. Hoedemaeker and E. Erba, pers. communs., 1993), and a stratigraphic age as young as earliest Valanginian Stage is possible. Nevertheless, we maintained the Berriasian Age assignment for this 137.1 Ma date. Therefore, its high-precision error limit constrains the Berriasian/Valanginian boundary to be not older than 137 Ma. The Berriasian/Valanginian boundary has been correlated to polarity chron M15n.4 (Ogg and others, 1988). The relative stratigraphic timing of an event within the polarity zone is denoted by using the appropriate fractional subdivision within the zone (modified from Hallam and others, 1985; Ogg and others, 1991a). Therefore, an event at "C33n.85" implies that 85% of normal-polarity chron C33n precedes the event. However, CK92 used this notation in opposite sense; therefore, C33n.15 in their notation denotes that 15% of polarity chron C33n followed the event.

Barremian/Aptian Boundary

Dates near the Barremian/Aptian boundary anchor the youngest part of the Hawaiian sequence of marine magnetic anomalies in magnetostratigraphy. Magnetic polarity chron M0r occurs in the Early Aptian *Chiastozyus litterarius* calcareous nannofossil Zone. The base of polarity zone M0r may coincide with the Barremian/Aptian Stage boundary (E. Erba, pers. commun., 1993).

Pringle (1995) obtains an Ar/Ar date at the top of polarity zone M1r in seamount basalts of MIT Guyot of 123.51 ± 0.5 Ma (1σ), which implies an age of approximately 121 Ma for the base of polarity chron M0r and the Barremian/Aptian boundary (Appendix 1, item 213).

Campanian/Maastrichtian Boundary

The former calibration of microfossil datums and magnetic polarity chronos to the macrofossil placement of the Campanian/Maastrichtian boundary has been revised upward.

The Campanian/Maastrichtian boundary was correlated to the top of the *Globotruncana calcarata* foraminiferal Zone in the Gubbio Section, Italy, and this datum occurs in the upper part of polarity zone C33n (C33n.85) (Alvarez and others, 1977).

This foraminiferal datum may be correlated to bentonites in the U.S. Western Interior, yielding K/Ar and Ar/Ar dates of 74.5 Ma, thereby providing a tie point for the Late Cretaceous magnetic polarity scale (Cande and Kent, 1992).

The base of the Maastrichtian is close to the appearance of *Belemnella lanceolata*, a well-defined belemnite datum in the boreal realm (Birkelund and others, 1984). In Kronsmoor, Germany, a suitable boundary stratotype for the Campanian/Maastrichtian boundary, *Belemnella lanceolata*, appears 3.5–5 m below *Hoploscaphites constrictus*, an ammonite datum also used for recognition of the Campanian/Maastrichtian boundary in the boreal realm.

Kennedy and others (1992) and McArthur and others (1993) have established detailed macrofossil and strontium isotope correlations, respectively, between the Kronsmoor section, the

Campanian/Maastrichtian boundary in the English Chalk and the Upper Campanian/Lower Maastrichtian of the U.S. Western Interior. Kennedy and others (1992) found that the top of the *Globotruncana calcarata* foraminiferal Zone occurs significantly older than the macrofossil assignment of the Campanian/Maastrichtian boundary. These studies also correlate the Campanian/Maastrichtian boundary in Kronsmoor to a level within the *Baculites jensi* ammonite Zone or possibly the overlying *Baculites eliasi* Zone in the United States Western Interior. The *Baculites jensi* Zone is in a series of eight *Baculites* zones spanning the Upper Campanian-Lower Maastrichtian of the Western Interior (Obradovich, 1988). The isotope correlations suggest a moderate uniformity of zonal duration from the *B. compressus* zone to the *Baculites grandis* Zone. Obradovich (1988) gives K/Ar ages for bentonites in the *B. grandis* Zone of 70.1 ± 0.7 Ma and for the *B. compressus* Zone of 73.2 ± 0.7 Ma. A linear interpolation results in an estimate for the Campanian/Maastrichtian boundary of 71.6 ± 0.7 Ma. This estimate closely matches that of PTS89 based on chronogram interpolations of 40 Maastrichtian and Campanian radiometric age dates and is the preferred one in our analysis (items 52, 53 and 56 in Appendix 1).

Therefore, the CK92 age of 74.5 Ma for a level in the upper part of polarity zone C33n is satisfactory for magnetostratigraphy but is not satisfactory for dating the Campanian/Maastrichtian boundary. Hicks (1993) correlated magnetic polarity zones C29n through C33r to ammonite zones in the United States Western Interior and interpolated ages for the magnetic reversals from the dated bentonite horizons (Obradovich, 1988, 1993). We combined these ages on the magnetic polarity chronos and associated error limits derived by Hicks (1993) with the spacing of magnetic anomalies in CK92 to obtain a best-fit, smoothed seafloor spreading curve and associated ages of the magnetic polarity chron boundaries.

Cretaceous/Paleogene Boundary

The Cretaceous/Paleogene (Cretaceous/Tertiary) or Maastrichtian/Danian boundary occurs in the upper portion of polarity chron C29r (approximately C29r.7), according to an average of 5 magnetostratigraphic sections (CK92). PTS89 obtained a chronogram age of 66 Ma for the K/T boundary, using 20 age dates for the Maastrichtian and 15 for the Danian. Obradovich (1988) arrived at the same 66 Ma value, based on a magnetostratigraphic section in Red Desert Valley, Alberta (item 31, Appendix 1). The 66 Ma age estimate was also supported by laser fusion $^{40}\text{Ar}/^{39}\text{Ar}$ dates (unpubl.) on single crystals of sanidine extracted from the iridium-bearing lower Z coal in Montana, which yielded a mean age of 66.1 Ma (C. Swisher, as cited by Berggren and others, 1992). However, these dates were later rejected as being analytically suspect (C. Swisher, pers. commun., 1993).

Our age of the Maastrichtian/Danian (Cretaceous/Paleogene) boundary combines the standardized Ar/Ar dates of 64.98 ± 0.05 Ma and 65.2 ± 0.4 Ma at the Chicxulub impact crater, with age estimates for the Arroyo el Mimbral (Mexico) and Beloc (Haiti) tektites of 65.07 ± 0.10 Ma and 65.01 ± 0.08 Ma (Swisher and others, 1992; Sharpton and others, 1992) to yield 65.00 ± 0.04 Ma (item 34 in Appendix 1).

MAXIMUM LIKELIHOOD ESTIMATION

The maximum likelihood method is suitable for estimation of the age of stage boundaries from a radiometric database if most rock samples used for age determination are subject to significant stratigraphic uncertainty. The method is particularly applicable where a group of radiometric dates with differing precision is available near, but not at, a stage boundary. It provides a way of combining the measurement errors of the dates with their stratigraphic uncertainty.

In the method of maximum likelihood, one or more parameters of a statistical population are estimated by maximizing the likelihood that a sample of observed values was drawn at random from the population. Each parameter to be estimated is considered as a variable in the equation of the frequency distribution for the population which has to be known beforehand. The frequency distribution of a maximum likelihood estimator itself converges to normal (Gaussian) form with increasing sample size.

A statistical model for the construction of chronograms was originally proposed by Cox and Dalrymple (1967). It is based on the following two assumptions: (1) the true ages of the rock samples subjected to radiometric age determination are uniformly distributed over time in the vicinity of the chronostratigraphic boundary of which the age is to be estimated (i.e., the number of dates per time interval remains constant on the average), and (2) each date is derived from a normal (Gaussian) distribution centered around the true age of the rock sample with the reported measurement error as its standard deviation. This model allows for a date to be inconsistent in two ways: a sample known to be stratigraphically younger than a given boundary may have a measured date that is older than the age of the boundary, and a stratigraphically older sample may produce a measured date that is younger.

PTS82 and PTS89 constructed chronograms in the following way. For a number of equally spaced test ages in the vicinity of a stage boundary, the sum of squares is computed for standardized differences between each test age and the dates that are inconsistent for it. Each difference is standardized by dividing it by the standard deviation of the date. The number of inconsistent dates for a test age increases when the test age becomes either significantly younger or older than the true age of the boundary that is to be estimated. The graph representing the relation between the sum of squares plotted in the vertical direction and the test age (horizontal axis) is a chronogram. Typically, a chronogram of this type resembles a basket with a relatively flat bottom around its minimum value which is selected as the best estimate of the age of the stage boundary. Updated chronograms were constructed for PTS89.

The preceding method can be improved by applying the method of maximum likelihood, using the consistent dates in addition to the inconsistent dates for each test date (Agerberg, 1988, 1990). If the two basic assumptions (uniform distribution of samples through time with superimposed Gaussian errors) hold true, the probability P_u that a date x_i with standard deviation σ_i differs from a given test age μ_t satisfies $P_u = 1 - \Phi(z_{it})$, where $z_{it} = (x_i - \mu_t)H_i/\sigma_i$ is the standardized date and Φ represents cumulative frequency of the normal (Gaussian) distribution in standard form. In the equation for z_{it} , H_i denotes stratigraphic relation between sample and boundary: $H_i = 1$ for

older samples and $H_i = -1$ for younger samples. The product of the probabilities, which may be written as πP_u , reaches its maximum for the test age which is closest to the true age.

The product of the probabilities also known as the likelihood function $L_t = \Pi P_u$ tends to become normal (Gaussian) as the number of independent observations increases. In general, the log-likelihood function $\log_e L_t = \Sigma \log P_u$, where Σ denotes summation, assumes a bell-shaped curve. This alternative form is more suitable for further calculations and is used for graphical representation in the log-likelihood graphs (see Fig. 6). A procedure commonly used is to locate the maximum of the log-likelihood function by means of the method of scoring (e.g., Rao, 1973) which involves a local, iterative search.

Inconsistent dates have negative values of z_{it} and result in values of P_u which are less than 0.5. For example, if an inconsistent date is three standard deviations away from a test age (i.e., $z_{it} = -3.0$ or $h_t - x_i = 3\sigma_i$), then $P_u = 0.00135$. A small value like this leads to a significant decrease in ΠP_u . On the other hand, consistent dates have positive values of z_{it} resulting in values of P_u which are greater than 0.5 but less than 1.0. For $z_{it} = 3.0$, $P_u = 0.99865$ which is nearly equal to 1.0. This implies that consistent dates more than three standard deviations away from a test age have almost no influence on the product ΠP_u . The standard deviations σ_i are the measurement errors of the dates.

When the number of dates is large, the maximum likelihood method gives approximately the same results as the method used in PTS89. However, when there are relatively few dates, as in the pre-Aptian time interval, use of the consistent dates yields significantly better results. Moreover, the method provides a standard deviation for the best estimate. Locally, the end product of maximum likelihood resembles a Gaussian curve of which the standard deviation can be determined and used as the standard deviation of the best estimate.

The maximum likelihood method was used to estimate the ages of 30 Mesozoic stage boundaries from the Permian/Triassic to the Cretaceous/Paleogene boundary (Table 1). Triassic through Albian estimates obtained by scoring applied to high-temperature dates (highlighted in Table 1) were later combined with other types of estimates (Table 2) for estimation of the 31 stage boundaries of the Mesozoic Era.

Local Versus Wider-Range Log-Likelihood Maxima

Initially, a trial age was selected for each boundary in order to define the subset of dates from the Mesozoic radiometric database as well as the sequence of test ages to be used for that boundary. The ranges for the dates and trial ages for the stage boundaries were set as follows. In the Late Cretaceous Period, all dates within 10 my from a prior estimate of the age of the stage boundary were used, and the corresponding range of the test ages was set half as wide (trial age ± 5 my). For the older stages, these two windows were set at trial age ± 20 my and ± 10 my, respectively. The trial ages, listed in the database of Appendix 1, are our best subjective estimates for the age of Mesozoic stage boundaries.

Log-likelihood graphs were constructed for all 30 stage boundaries estimated (see Fig. 6). The method of scoring was applied to locate the maxima of the log-likelihood functions. These estimates (m) are shown in Figure 6 with their 95% con-

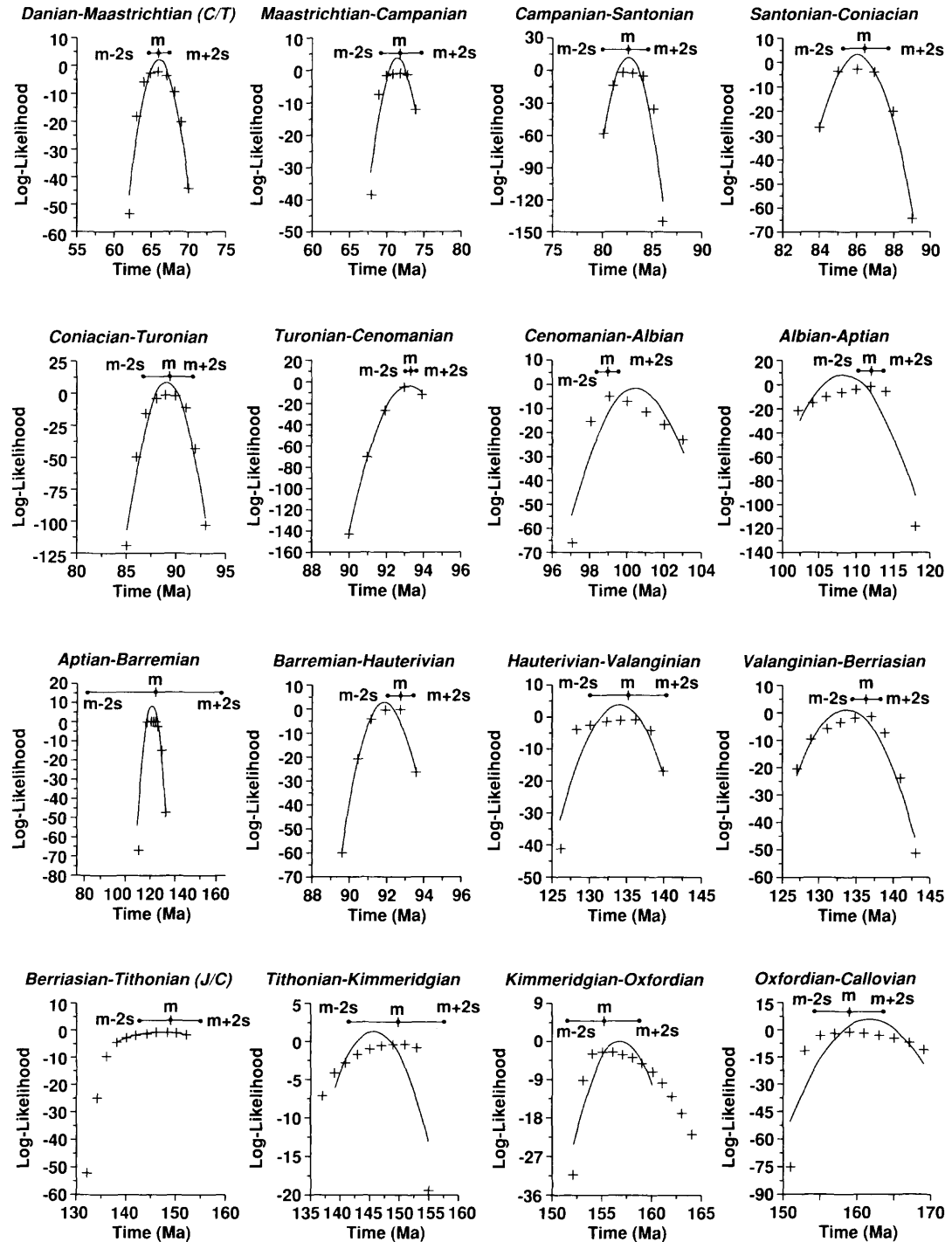


FIG. 6.—Log-likelihood plots for 30 Mesozoic stage boundaries (high-temperature dates). Log-likelihood is plotted against test ages in geological time. Lack of data prevented using maximum likelihood estimation for the Induan-Olenekian boundary. Largest log-likelihood value (m) and corresponding standard deviation (σ) found by method of scoring were used for approximate 95% confidence intervals ($m \pm 2\sigma$). Parabolas were fitted to log-likelihood values for wider neighborhoods around prior estimates (trial ages). Each parabola provides other estimates: m_p (parabola peak) and σ_p (parabola standard deviation). Asymmetry of the log-likelihood function results in differences between m and m_p ; and $\sigma > \sigma_p$, if the likelihood function has a flatter peak than the parabola; in Table 1, σ is replaced by σ_p for the Barremian-Aptian boundary which is exceptionally flat. These types of discrepancies are primarily due to the influence of relatively few recent dates that are much more precise than the earlier dates.

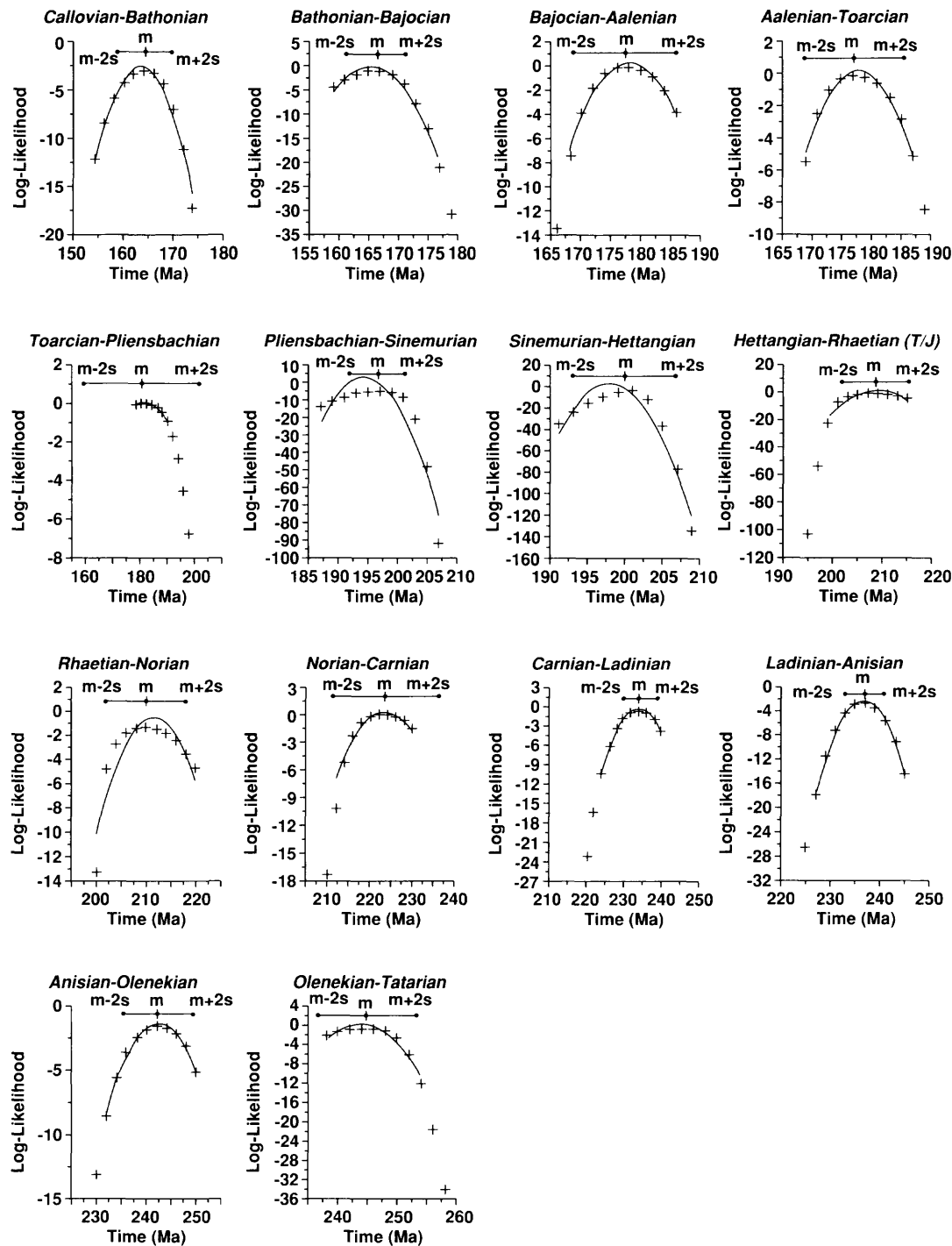


FIG. 6.—Continued.

fidence interval ($m \pm 2\sigma$). Scoring is equivalent to constructing a parabola through three points over a very narrow range at the peak of the log-likelihood function. Additionally, parabolas were fitted to the likelihood values from wider ranges defined by the test ages by using the method of least squares. An advantage of this replacement of the calculated log-likelihood values by a continuous curve may be to reduce the effect of local (random) fluctuations. The peaks of the parabolas also can be

used to estimate the stage boundary ages. In all cases scoring and parabola-fitting methods gave approximately the same age, but the corresponding standard deviations are only approximately equal if the parabola provides a good fit to the log-likelihood function.

In most graphs, the log-likelihood function has a flatter top than the best-fitting parabola and asymmetry occurs in some graphs (e.g., Hauterivian/Barremian, Valanginian/Hauterivian,

TABLE 2.—STEPWISE CALCULATION OF MESOZOIC TIME SCALE

Stage	Individual Age Estimates		Spline Computations		
	Initial ^a	Modified ^b	Ages ^c	Deviations ^d	Final Ages ^e
Maa	65.00 ± 0.04			65.0 ± 0.1	
Cam	71.30 ± 0.25	71.29 ± 0.25		71.3 ± 0.5	
San	83.50 ± 0.25	83.46 ± 0.24		83.5 ± 0.5	
Con	86.30 ± 0.25	85.79 ± 0.23		85.8 ± 0.5	
Tur	88.70 ± 0.25	88.96 ± 0.25		89.0 ± 0.5	
Cen	93.30 ± 0.10	93.49 ± 0.08		93.5 ± 0.2	
Alb			(0.30 0.31)	98.9 ± 0.6	
Apt			(0.87 0.53)	112.2 ± 1.1	
Bar	120.77 ± 0.50	120.98 ± 0.41	(0.41 0.69)	121.0 ± 1.4	
Hau	126.93 ± 1.00	127.03 ± 0.66	(0.66 0.81)	127.0 ± 1.6	
Val	132.03 ± 1.00		(1.00 0.94)	132.0 ± 1.9	
Ber	138.36 ± 1.50	136.99 ± 0.81	(0.81 1.08)	137.0 ± 2.2	
Tit	144.19 ± 1.50		(1.50 1.31)	144.2 ± 2.6	
Kim	150.69 ± 1.50		(1.50 1.52)	150.7 ± 3.0	
Oxf	153.46 ± 2.00	154.36 ± 1.34	154.10	154.1 ± 3.2	
Cal	159.99 ± 2.00	159.59 ± 1.51	159.36	159.4 ± 3.6	
Bat			164.43	164.4 ± 3.8	
Baj			169.20	169.2 ± 4.0	
Aal			176.54	(2.02)	176.5 ± 4.0
Toa			180.08	(2.02)	180.1 ± 4.0
Pli			189.63	(1.98)	189.6 ± 4.0
Sin			195.27	(2.23 1.96)	195.3 ± 3.9
Het			201.89	(0.67 1.97)	201.9 ± 3.9
Rha			205.66	(1.65 2.00)	205.7 ± 4.0
Nor			209.59	(2.61 2.06)	209.6 ± 4.1
Car			220.74	(3.02 2.21)	220.7 ± 4.4
Lad			227.40	(2.22 2.27)	227.4 ± 4.5
Ani	232.62 ± 2.76	235.21 ± 1.60	234.29	(1.73 2.32)	234.3 ± 4.6
Ole			241.66	(2.81 2.36)	241.7 ± 4.7
Ind			244.82	(2.38)	244.8 ± 4.8
Tat	248.18 ± 0.28	248.16 ± 0.28	248.20	(2.22 2.40)	248.2 ± 4.8

Standard deviations in parentheses except in last column for final age with estimated 2σ precision. Selected maximum likelihood results in Table 1 (see footnote) were combined with other estimates.

^aInitial estimates for Cretaceous-Cenozoic boundary (Maa), OB93 (Cen-Cam), Hawaiian magnetostratigraphy (Cal-Bar), and direct estimates for Tat and Ani.

^bFinal estimates for Middle-Late Cretaceous. Other modified estimates (Tat-Bar) are averages of direct estimates of column 2 combined with maximum likelihood estimates of Table 1.

^cSmoothing and interpolation results obtained by spline-curve fitting.

^dInput and output for separate spline-curve fitted to standard deviations.

^eFinal ages with 2σ-precision.

and Berriasian/Valanginian boundaries in Fig. 6). These discrepancies are due to local scarcity of dates and sensitivity of the method to relatively few, more recent dates that have a standard deviation which is much smaller than the majority of the dates used; also, the frequency distribution of the ages of the dated samples is not everywhere approximately uniform, and this results in asymmetric log-likelihood functions. The validity of these statements is illustrated by using computer simulation experiments (Agterberg, in press). A comparison between estimates for the wider-range (parabola) and local (scoring) maxima is given in Table 1 for high-temperature dates only.

Estimates based on situations where the parabola provides a good fit to the log-likelihood function are the best. In the other cases, the parabolas fitted to the chronograms provide answers that are fairly good approximations. In all cases, the position of the local (scoring) maximum was taken as the best estimate of the mean. Several of the estimates, especially in the Jurassic, have relatively large standard deviations due to scarcity of dates and were not used (e.g., Valanginian/Hauterivian, Aalenian/Bajocian, and Toarcian/Aalenian boundaries in Fig. 6).

For high-temperature dates, the largest deviations (those >2 my) in location of the peak of the best-fitting parabola occur at the upper stratigraphic boundary of Kimmeridgian (~4.1 my),

Aptian (~3.9 my), Callovian (2.8 my), Berriasian (~2.7 my), Hettangian (~2.7 my), and Hauterivian (~2.2 my). Most of these differences are negative with the parabola peak older than the local maximum. In part, this reflects asymmetry of the log-likelihood function caused by decreasing frequency of dates toward older stages. The local maximum provides a better estimate than the parabola peak in all cases. Most standard deviations for local maxima as derived by the scoring method are greater than those based on the parabolas. This is because approximate normality of the likelihood function has not been reached because of insufficient data or order of magnitude differences in precision of individual age estimates, and most local maxima remain flatter than the peaks of the wider-range parabolas. Consequently, most standard deviations obtained by scoring are slightly too large.

High-Temperature Versus Low-Temperature Dates

Three maximum likelihood functions were developed for each boundary (Table 1). Unless there were insufficient data, high- and low-temperature dates were analyzed separately as well as combined. Dates determined by methods and materials with closure temperature less than 250°C (cf. Harland and others, 1990, Table 4.1) were classified as low-temperature dates. These are reset more readily than high-temperature dates. The low-temperature dates are almost exclusively K/Ar dates on glauconites with closure temperature of about 200°C. Probabilities that the low-temperature mean is younger than the high-temperature mean were computed as follows. For each boundary, the low-temperature estimate was subtracted from the high-temperature estimate. The resulting number was divided by the combined standard deviation for the two estimates. The resulting standardized value was converted into the probability that the low-temperature estimate is younger than the high-temperature estimate (one-tailed significance test). As shown in Table 1, ten successive maximum likelihood estimates based on low-temperature dates from top Cenomanian downward are significantly younger with probability greater than 99%.

The systematic discrepancy between high-temperature and low-temperature estimates fluctuates between 3 my and 18 my. The preceding, statistical significance test merely indicates that, on the average, either the low-temperature dates are too young, the high-temperature dates are too old, or both these test hypotheses could be true. We have assumed that only the high-temperature dates are unbiased. From top Callovian downward, there are very few low-temperature dates, and the maximum likelihood estimates are not changed significantly whether or not these low-temperature dates are included (Table 1, column 5). For all boundaries, only the high-temperature estimates were used.

Within the Mesozoic Era, the systematic difference between high- and low-temperature estimates is restricted to the time interval between the Oxfordian and the Santonian Stages. This bias was not found in the younger stages where low-temperature dates are abundant nor in the older stages where they are scarce. This indicates that the problem of bias is not related to choice of decay constants. The low-temperature dates are primarily K/Ar dates for glauconites and may provide minimum ages instead of unbiased estimates. This topic is discussed in more detail in other publications (e.g., Gradstein and others, 1988; Harland and others, 1990).

CALLOVIAN THROUGH BARREMIAN MAGNETOCHRONOLOGY

The magnetic anomaly record of the oceanic crust coupled with magneto-biostratigraphic correlations provides a powerful means for relative scaling of the durations of the associated geological stages (e.g., Cande and Kent, 1992). Estimates of the ages of biostratigraphic datums and stage boundaries are possible once the magnetic anomaly scale has been pinned to several radiometric tie points.

This scaling procedure is not possible for the middle portion of the Cretaceous because a long interval of normal polarity, the "Cretaceous Long Normal-Polarity Chron" or polarity chron C34n, extends from the early Aptian to the Santonian/Campanian boundary. Within the late Aptian through late Albian portion of the Cretaceous Long Normal-Polarity Chron, brief subchrons of reversed-polarity have been observed in pelagic sediment sections although there are no well-defined marine magnetic anomalies recognized in ocean crust of these ages (reviewed by Ogg, 1995).

The spacing of the Hawaiian sequence of marine magnetic anomaly lineations M0 through M25 is used here to interpolate the Oxfordian-Aptian time interval and arrive at ages for the intervening stage boundaries. The same procedure was utilized by the DNAG scale (Palmer, 1983; KG85). This "M-sequence" of polarity chronos M0r through M25r is from the Larson and Hilde (1975) model with nomenclature after A. V. Cox (in PTS82) and with a brief reversed-polarity subchron inserted in M11n (Tamaki and Larson, 1988).

Cande and others (1978) identified a series of Jurassic magnetic anomalies in the western Pacific, which they called M26 through M29. Later, Handschumacher and others (1988) used more detailed surveys to propose a revised M26 through M38 pattern, which retained in modified form the M26–M28 portion from Cande and others (1978) and extended the series by approximately 5 my. Handschumacher and others (1988) assigned ages to their M26–M38 pattern by assuming a constant spreading rate from M21–M38 in the Japanese lineations and using the M21–M25 ages of Larson and Hilde (1975) scale.

The anomaly numbering of Handschumacher and others (1988) was retained in this new scale, but their polarity chron nomenclature was revised to be consistent with the younger portion of the M-sequence (nomenclature system of Cox). Therefore, subchrons are labeled according to whether they are subdivisions of a major normal-polarity chron or of the underlying reversed-polarity chron. For example, the normal-polarity chron "35a" of Handschumacher and others (1988) is labeled as subchron "M35r.1n" occurring within reversed-polarity chron M35r. There may be a one-chron duplication within the marine magnetic anomaly pattern of Handschumacher and others (1988) due to a spreading ridge jump (R. Larson, pers. commun., 1991).

Correlation of the M-sequence polarity chronos to ammonite, calcareous nannofossil, dinoflagellate and calpionellid zones and datums are compiled by Ogg (1988, 1995), Bralower and others (1989) and Ogg and others (1991a). Additional magnetostratigraphy studies within Lower Cretaceous strata (e.g., Channell and Erba, 1992) have indicated that further refinement of stage boundary positions relative to the magnetic polarity pattern is constrained by the use of micropaleontological markers rather than ammonite zones to recognize stage boundaries

and by the variable preservation and reworking of those micropaleontological markers.

The Barremian/Aptian boundary is correlated to the base of polarity chron M0r. This magnetostratigraphic correlation, which is under consideration by the Subcommission on Cretaceous Stratigraphy (E. Erba, pers. commun., 1993), is only slightly older than the magnetochronologic placement in previous scales (e.g., KG83).

The Hauterivian/Barremian stage boundary occurs approximately two-thirds from the base of polarity chron M5n (M5n.66; Cecca and others, 1994). Previous magnetic polarity time scales had placed this boundary near polarity chron M7 based on microfossil assignments, but these microfossil datums and associated polarity chron ages have now been recalibrated to ammonite zones.

There have not been any precise ammonite or nannofossil markers for the Valanginian/Hauterivian boundary in magnetostratigraphic sections, and the observed variability in the dinoflagellate marker (last appearance datum of *Scriniodinium dictyotum*) brackets polarity zone M10Nr. Therefore, we provisionally assign this boundary to the middle of polarity chron M10Nr.

The base of the *Thurmanniceras pertransiens* ammonite Zone in southern Spain occurs just below the middle of polarity chron M15n, and the corresponding Berriasian/Valanginian Stage boundary is placed at M15n.4.

The Tithonian/Berriasian stage boundary at the base of the *Berriasella jacobi* Zone is in the upper portion of polarity chron M19n (approximately M19n.2n.5; Ogg and others, 1991a).

The base of the *Hybonoticeras hybonotum* ammonite Zone is the Kimmeridgian/Tithonian boundary. This horizon occurs in southern Spain within polarity chronos M23n to M22An (Ogg and others, 1984). In this study, the boundary is assigned to the top of polarity chron M23n.

The base of the *Sutneria platynota* ammonite Zone appears to occur within polarity chron M25r or M24Br within southern Spain (Ogg and others, 1984). Therefore, pending detailed magnetostratigraphic studies, a working definition for the Oxfordian/Kimmeridgian boundary is the top of polarity chron M25n.

Close-spaced magnetic anomalies M26 through M39 are observed in Pacific crust of presumed Early Callovian-Oxfordian Age (Handschoenmacher and others, 1988). Magnetostratigraphy of Callovian-Oxfordian sections have also indicated rapidly changing polarity (Steiner and others, 1986; Channell and others, 1990; Ogg and others, 1991b). However, the correlation of the Callovian/Oxfordian boundary to the magnetic anomaly sequence remains ambiguous. Pre-M39 oceanic crust in the Pacific is called the "Jurassic Quiet Zone," and the indistinct nature of the oceanic crust magnetization of this region may indicate the blurring effect caused by a high frequency of magnetic reversals. Ocean Drilling Program (ODP) Site 801 was drilled in oceanic crust older than magnetic anomaly M39, and the basement basalts are dated by radiolarian assemblages as latest Bathonian or earliest Callovian (Larson, and others, 1992).

The ages of these stage boundaries can be estimated by assuming a constant rate of spreading of the Hawaiian magnetic anomaly lineations during the Late Jurassic and Early Cretaceous Periods. There are only two direct radiometric datings of magnetic anomalies: (1) the top of magnetic polarity zone M1r

as 123.5 ± 0.5 Ma at ODP Site 878 on MIT guyot basalts (M. Pringle, pers. commun., 1993, 1995) and (2) magnetic anomaly M26r as 155.3 ± 3.4 Ma at ODP Site 765 in the Argo Abyssal Plain (Ludden, 1992). These tie points were used to project the ages of the magnetic polarity chronos associated with the stage boundaries:

Barremian/Aptian	120.77 Ma
Hauterivian/Barremian	126.93
Valanginian/Hauterivian	132.03
Berriasian/Valanginian	138.36
Tithonian/Berriasian	144.19
Kimmeridgian/Tithonian	150.69
Oxfordian/Kimmeridgian	153.46

Magnetostratigraphy does not easily allow an estimate of uncertainty since no error is available for the seafloor lineations distances, or for the age estimates of the tiepoints (e.g., Cande and Kent, 1992). We have assigned arbitrary uncertainties on these constant-spreading estimates based upon the standard deviations of the ages on the magnetic polarity chron M1r and M26r tie points (Appendix 1).

These ages derived from a constant spreading rate assumption must be reconciled with the radiometric databases and associated maximum likelihood age estimates. For this purpose, we performed a weighted average of the boundary age estimates obtained independently from the constant spreading rate model and the maximum likelihood. For the Barremian/Aptian, Hauterivian/Barremian, and Oxfordian/Kimmeridgian boundaries, the maximum likelihood ages are essentially identical as the ages from the constant spreading rate model, indicating that the choice of the two age tie points for the Hawaiian lineation scaling are consistent with the radiometric database as a whole. For the Kimmeridgian/Tithonian/Berriasian boundary suite and the Valanginian/Hauterivian boundary, where there are so few high temperature radiometric ages that the maximum likelihood age estimates for the adjacent boundaries overlap (Table 1), the spreading rate estimates and uncertainties were used exclusively for the boundary age interval for the following spline fit.

However, for the Berriasian/Valanginian boundary, the maximum-likelihood age estimate is significantly older than the estimate based on the constant spreading-rate model (Table 1). This suggests that the spreading rate for the Berriasian may be slower than during the Valanginian stage. As explained in the next section, further scaling using spline-fitting of the age sets, supports the interpretation that the average spreading rate for the latest Jurassic and earliest Cretaceous Periods was slower than during the Valanginian-Hauterivian-Barremian stages.

COMBINING MAXIMUM LIKELIHOOD AND MAGNETOCHRONOLOGY RESULTS

The next step in time scale calculation was to combine the Triassic-Early Cretaceous maximum likelihood age estimates with direct ages estimates of stage boundaries based on Oxfordian-Aptian magnetostratigraphy and with direct estimates for the Olenekian/Anisian and Permian/Triassic boundaries. This approach of weighted averaging combines stratigraphic and mathematical interpolations on the age of those stage boundaries for which no detailed, high-resolution geochronologic estimate is available similar to that for Late Cretaceous time.

A basic assumption underlying the maximum likelihood method is that the dates are randomly distributed over time in the vicinity of each stage boundary. This uniform distribution is assumed to be independent of the age of the stage boundary. On the other hand, direct estimates of stage boundary ages are available in a number of situations. These direct estimates are either dates for samples that were almost exactly taken at a given stage boundary or those derived from magnetostratigraphic correlation of a stage boundary to a calibrated seafloor spreading model. Provided that the direct estimates are independent and were not used for constructing the maximum likelihood graph, they may be combined with one another and the maximum likelihood estimate by assuming that a single overall mean age for the stage boundary is being estimated.

Suppose that n estimates X_j ($j = 1, \dots, n$) with variances σ_j^2 are to be combined into a single estimate $X = \sum w_j X_j$, where the coefficients w_j are relative weights. It can be shown (e.g., Deming, 1948) that the optimum choice of weights is $w_j = \sigma_j^{-2}/\sum \sigma_j^{-2}$. The variance of X then satisfies $\sigma^2(X) = \sum w_j \sigma_j^2$ (also see Taylor, 1982). This procedure was followed to combine the maximum likelihood estimates (Table 1, column 3) with those from Oxfordian-Aptian magnetostratigraphy, the Olenekian/Anisian boundary, and the Permian/Triassic boundary (Table 2, column 2). The results obtained this way are shown in Table 2, column 3.

Due to a general lack of radiometric dates for Early Triassic and Early and Middle Jurassic time, the corresponding absolute time scale is poorly constrained by the maximum likelihood method. For these intervals, a secondary scaling using relative numbers of biostratigraphic subdivisions provided improved age estimates of stage boundaries (Fig. 7). This secondary scaling is based upon high-resolution ammonite zonal subdivisions.

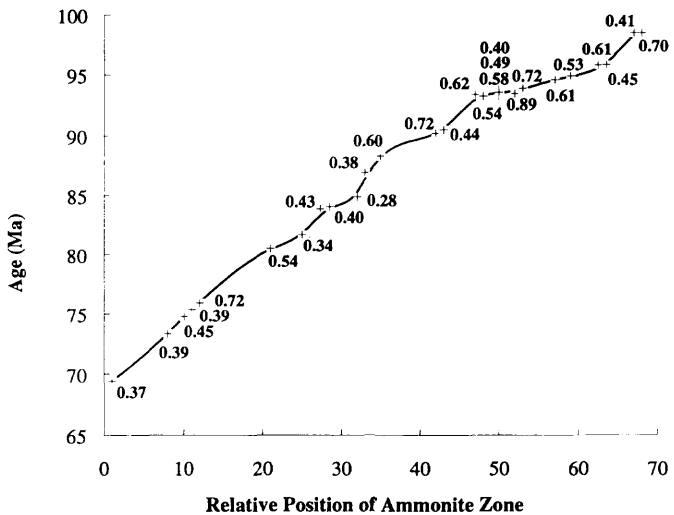


FIG. 7.—Cubic smoothing spline fitted to 27 $^{40}\text{Ar}/^{39}\text{Ar}$ dates (shown as '+'s with 2 σ -values) from Obadovich (1993) for bentonites in 25 biozones, United States Western Interior. These biozones belong to a continuous sequence of 65 biozones extending from the base of the mid-Cenomanian to the middle of the early Maastrichtian time. The bentonites were spaced assuming equal duration of these 65 biozones. This interpolation gave precise results because the standard deviations of the 27 dates are relatively small, ranging from 0.14 to 0.45 my, and the observations nearly fall on a continuous curve.

MESOZOIC AMMONITE ZONATION CALIBRATION

Mesozoic stages are traditionally recognized by ammonite zonal boundaries. Considerable consensus exists between specialists in different geographic areas of Europe about the placement of ammonite zones in particular stages although some ambiguity remains, especially in the lower Cretaceous Period. Only a few Mesozoic stage boundaries have been formally defined by a boundary stratotype.

The ammonite zonation calibrated here with the time scale (Fig. 8) is from "The Mesozoic-Cenozoic Chronostratigraphic Framework" (Hardenbol and others, in de Graciansky and others, Mesozoic-Cenozoic Sequence Stratigraphy of European Basins, SEPM Special Publication, in prep.) and represents a highest-resolution composite made up of the greatest number of ammonite zones or subzones described from any Mesozoic stage in Boreal or Tethyan areas of Europe. In addition, some upper Cretaceous high-resolution data from the Western Interior of the United States and Triassic data from British Columbia in Canada and of Siberia are included to supplement the western European data. The number of ammonite zonal units for each stage is listed in Appendix 1.

Since few ammonite zones are directly dated by radiometric methods, all zonal units within a stage have been arbitrarily assigned equal duration unless data were available to demonstrate otherwise. For example, the relative thicknesses of ammonite zones in outcrop may reflect either relative duration or rates of deposition. Exceptions to this equal-duration scaling are in portions of the Late Cretaceous where several Western Interior ammonite zones are well dated (Obradovich, 1993) and in the Kimmeridgian to Valanginian interval where calibrations with the magnetic polarity history are available (e.g., Ogg and others, 1991a).

Triassic Period

The Triassic ammonoid zonation has seen several important changes since the publication of Zapfe (1983), reflecting the improved knowledge of the Tethyan (Alpine) as well as Boreal Triassic sequences. For the Tethyan area, the subdivision of Krystyn (as cited by Zapfe, 1983) has been applied. Krystyn's subdivision has remained relatively unchanged as far as it concerns the Lower Triassic Period, but it is considerably modified in the Anisian, Ladinian and lowermost Carnian Stages following the zonation proposed by Mietto and Manfrin (cited in De Zanche and others, 1993). De Zanche and others (1993) used this zonation as a tool for their sequence stratigraphic subdivision of the Triassic in the Italian Dolomites. In the Alpine Triassic sequence, the lower part of the Anisian Stage contains no ammonoid assemblages. A detailed subdivision for the lower Anisian Stage is in Bucher (1989), who reported on the ammonoid succession from beds straddling the Spathian/Anisian boundary in Nevada, but the implications for correlations of these results are not fully understood (compare, e.g., Dagys, 1988).

The placement of the Anisian/Ladinian boundary in the Alpine Triassic strata is subject to a thorough re-evaluation (cf. Gaetani, 1993a, b). The boundary between the Anisian and Ladinian stages is placed at the base of the *Nevadites* Zone, following Krystyn (as cited by Zapfe, 1983). Brack and Rieber (1993), however, propose a redefinition of the Anisian/Ladinian bound-

ary at the base of the *Eoprotrachyceras curioni* Zone, a similar level as in the Boreal Triassic (cf. E. Tozer, cited in Zapfe, 1983). Mietto and Manfrin (cited in De Zanche and others, 1993) add the *Daxatina cf. canadensis* Subzone to their *Trachyceras* Zone and suggest an earliest Carnian Age for this subzone. Pending an internationally accepted decision on the Ladinian/Carnian boundary, the *Trachyceras aon* Zone is taken as the base of the Carnian Stage (cf. L. Krystyn, cited in Zapfe, 1983). This implies that the *D. canadensis* Subzone is provisionally retained in the Late Ladinian Stage. The rest of the Carnian subdivision follows L. Krystyn (as cited in Zapfe, 1983). The *Tropites dilleri* Zone is assigned a similar status as most of the Carnian, Norian and Rhaetian zones, each comprising two or more zonal units. The same reasoning is followed for the Norian, where the assemblages recognized by Tozer (as cited by Zapfe, 1983) are applied for the unit subdivision. The lower boundary of the Rhaetian Stage is provisionally taken at the base of the *Sagenites reticulatus* Zone (Gaetani, 1992). We consider the three ammonoid zones that constitute the Rhaetian, as being of equal status to those in the Carnian and Norian Stages, and hence, comprise each of two units.

Considerable progress has also been made in refinement of the biostratigraphic subdivision of the Boreal Triassic strata. Dagys and Weitschat (1993) provide an up-to-date discussion concerning the ammonoid and pelecypod zones of the Boreal Triassic strata, comprising Siberia, Svalbard (Spitsbergen), the Sverdrup Basin, and British Columbia. The Lower Triassic sequence of Siberia provides most of the units for the time scale. Tozer (as cited by Zapfe, 1983) subdivided the *Wasatchites tardus* Zone in two assemblages, each constituting one zonal unit.

We follow Dagys and Weitschat (1993) for the subdivision of the Spathian into four zones but refrain from applying the very detailed subdivision, which would imply assigning ten units for the Spathian alone.

For Middle Triassic units, the Siberian succession provides optimum resolution (Weitschat and Dagys, 1989), with a subdivision of the *Grambergia talmyrensis* Zone into four subzones. One of the subzones, *Karangites evolutus*, has been recognized on Spitsbergen (Weitschat and Dagys, 1989), supporting its correlative value. Dagys and Weitschat (1989) propose an improved correlation between Anisian ammonoid zones of the Boreal succession and British Columbia, particularly affecting correlation of the *deleeni* and *chischa* Zones. In the Boreal Triassic sequences, the Anisian/Ladinian boundary is taken at the base of the *Eoprotrachyceras subasperum* Zone (Tozer, 1967; Tozer in Zapfe, 1983). This level corresponds to the base of the *E. curioni* Zone in the Alpine Triassic strata. Units in the Upper Ladinian are derived from the nathorstid ammonoid zonation described from Siberia (Dagys and Konstantinov, 1992). Dagys and others (1993) reported new data concerning the Ladinian/Carnian boundary in the Boreal Triassic strata, proposing the *Nathorstites lindstromi* Zone as the first Ladinian ammonoid zone, including the *Daxatina canadensis* Zone on Bear Island (Svalbard). Dagys and others (1993) subdivide the lowermost Carnian *Stolleyites tenuis* Zone into two subzones, in Siberia as well as in Svalbard. Dagys and Weitschat (1993) propose an improved correlation of the Carnian and Norian ammonoid and bivalve zones between Siberia and British Columbia. As mentioned earlier, Upper Norian and Rhaetian ammonoid zones are given the same status as those in

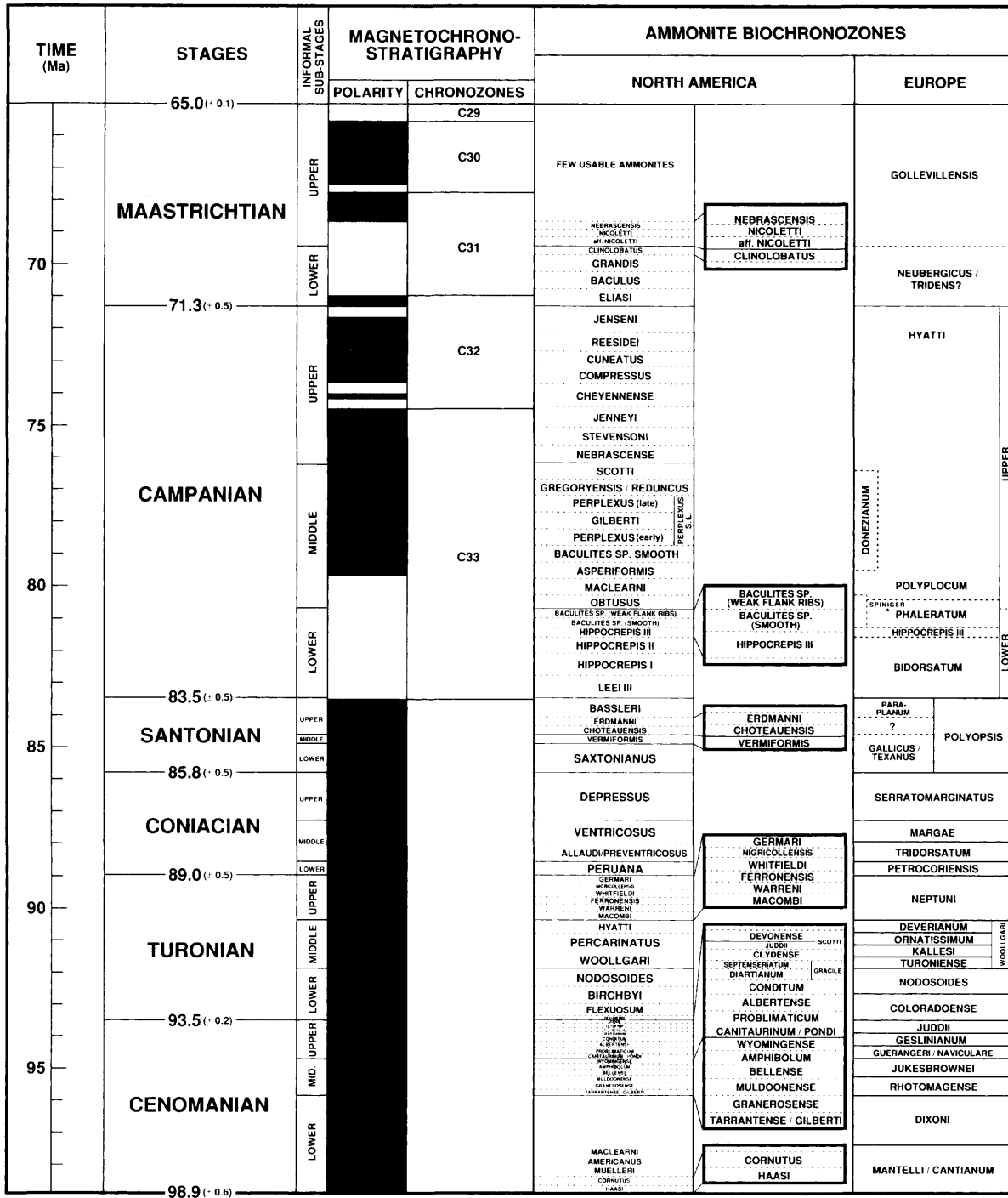


FIG. 8.—Highest-resolution Mesozoic ammonite subdivisions and magnetic polarity time scale calibration with North American and European highest resolution ammonite subdivisions. Direct calibration between ammonites and polarity exists for the middle Campanian through lower Maastrichtian stages (Hicks, 1993). North American ammonite calibration from Cobban and others (1994) and Obradovich (1993), European ammonites from J. M. Hancock (pers. commun., 1994) and F. Amédro (pers. commun., 1994).

the Norian and Carnian Stages, although no subzones have been recognized in this interval. Support for this practice is found in Kazakov and Kurushin (1992), who, based upon new finds from Siberia, subdivided the traditional Norian bivalve zones, such as the *Monotis ochotica* Zone, into several subzones.

Caution should be used when correlating the ammonoid zones between the Boreal and Tethyan Triassic strata. Due to endemism in each faunal realm, a direct comparison through correlation of different assemblages often is difficult. Only through integration of all zonal disciplines (e.g., zonations

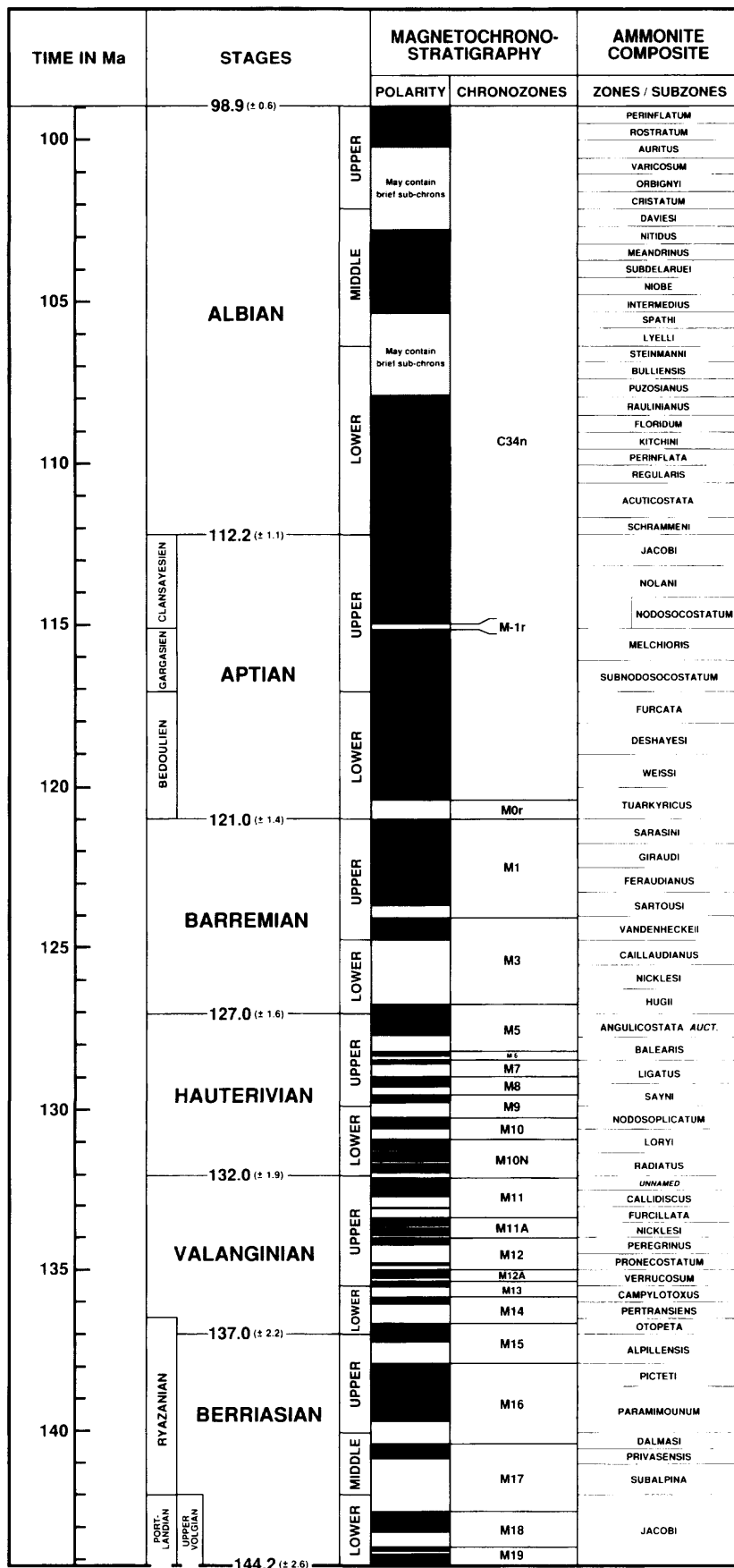


FIG. 8.—(B) Lower Cretaceous magnetic polarity time scale comparison with European highest-resolution ammonite subdivisions (Hoedemaker and others, 1993). Ammonites are calibrated with standard stages and the magnetic polarity history in the Berriasian and lower Valanginian. For the upper Valanginian through Albian, ammonites zones are calibrated with the stages only and are assumed to have equal duration with each stage.

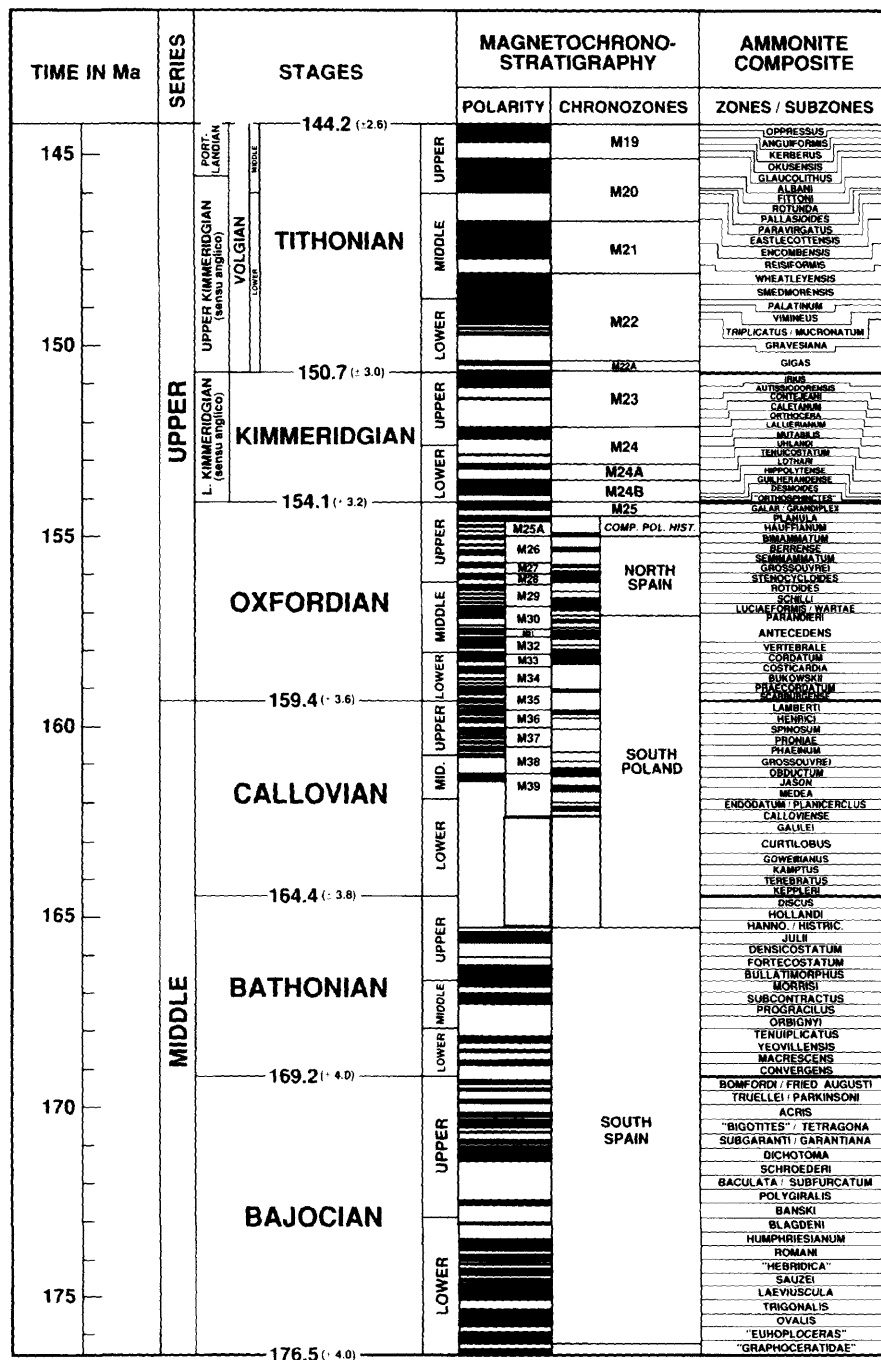


FIG. 8.—(C) Upper and upper Middle Jurassic magnetic polarity time scale comparison with European highest-resolution ammonite subdivisions from Boreal and Tethyan regions. Ammonites are calibrated with standard stages and the magnetic polarity history in the Kimmeridgian and Tithonian stages. For the Bajocian through Oxfordian stages, ammonite zones are calibrated with the stages only and are assumed to have equal duration within each stage.

based on conodonts and palynomorphs) and magnetic reversals will it be possible to understand the mutual relationship. Attempts to apply sequence stratigraphic correlations between widely different areas should bear in mind this limitation.

Direct calibration of magnetostratigraphy to ammonite zones has been accomplished in portions of the Early Triassic (Ogg and Steiner, 1991), Middle Triassic (Muttoni and others, 1994), and Late Triassic strata (Gallet and others, 1992, 1993; Marcoux, 1993).

Jurassic Period

Following the Tethyan convention the Jurassic/Cretaceous boundary is placed between the Tithonian and Berriasian stages. The boreal Portland and Volgian regional stages overlap a portion of the Berriasian stage (Fig. 8B–C). The Jurassic System is subdivided into a high-resolution “composite” of 180 units or subzones. The “composite” is made up of zones and sub-zones from Boreal as well as Tethyan areas to achieve maximal

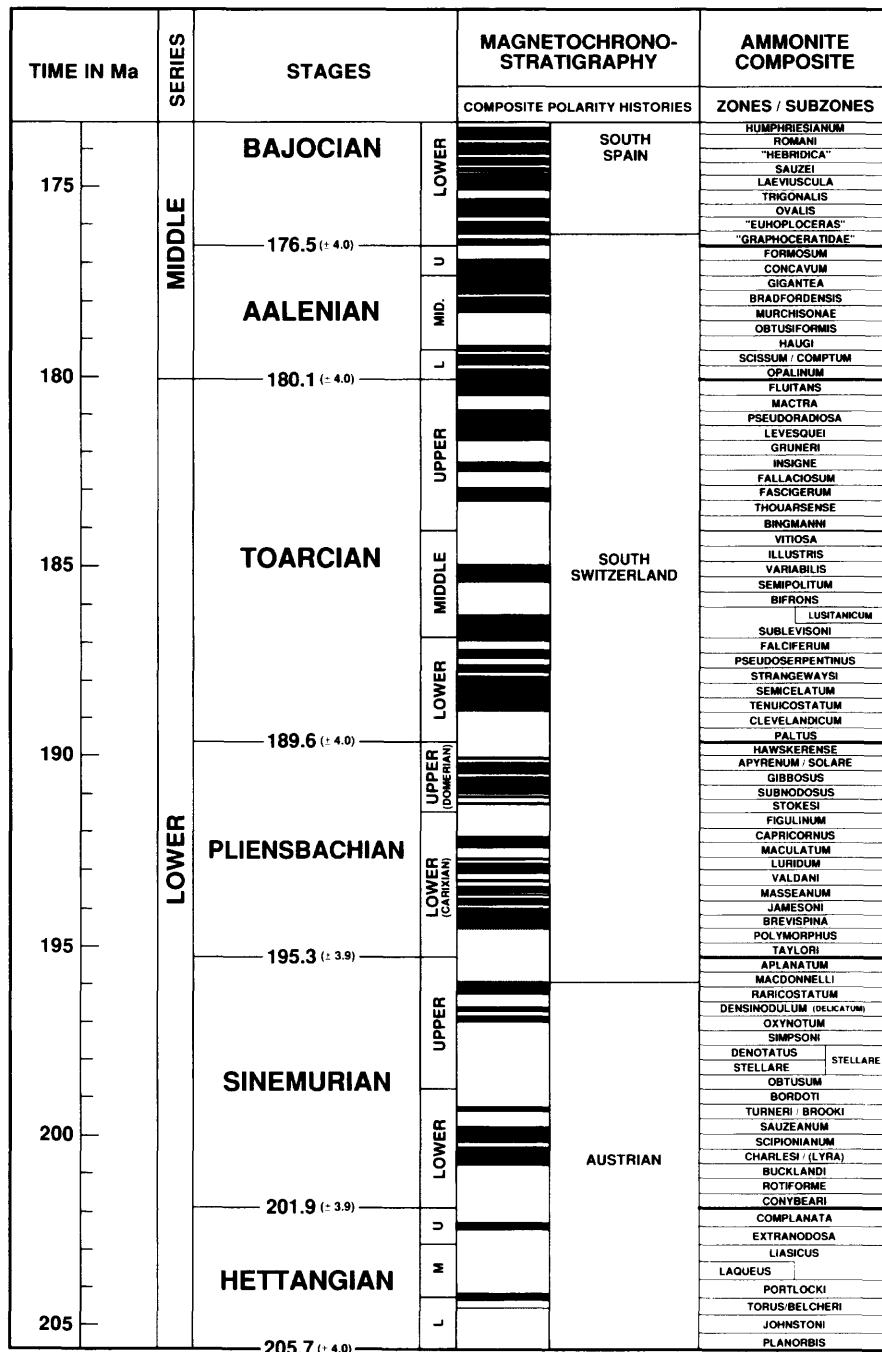


FIG. 8.—(D) Lower and lower Middle Jurassic magnetic polarity time scale comparison with European highest-resolution ammonite subdivisions from Boreal and Tethyan regions. Ammonite zones are calibrated with the stages only and are assumed to have equal duration within each stage.

resolution since no individual basin or region appears to provide high resolution throughout the Jurassic Period. The principal references for the composite zonation are Cope and others (1980a, b) and the Groupe Français d'Etudes du Jurassique (1991). A more comprehensive historic review of the Jurassic ammonite subdivisions and a calibration of Boreal and Tethyan zonal schemes is given in Hardenbol and others (in prep.). For the Hettangian through Oxfordian Stages, all ammonite zones/subzones in the composite zonation have been assigned equal

duration since no unambiguous information is available to decide otherwise. For the Kimmeridgian through Tithonian Stages, paleomagnetic calibration provided independent information for ammonite zonal durations (Ogg and others, 1984; Bralower and others, 1989; Ogg and others, 1991a).

The magnetic polarity pattern for several ammonite zones prior to the Kimmeridgian Stage is partially known. We have used the composite scale compiled by Ogg (1995), but with the Toarcian magnetic polarity pattern derived from a revised bio-

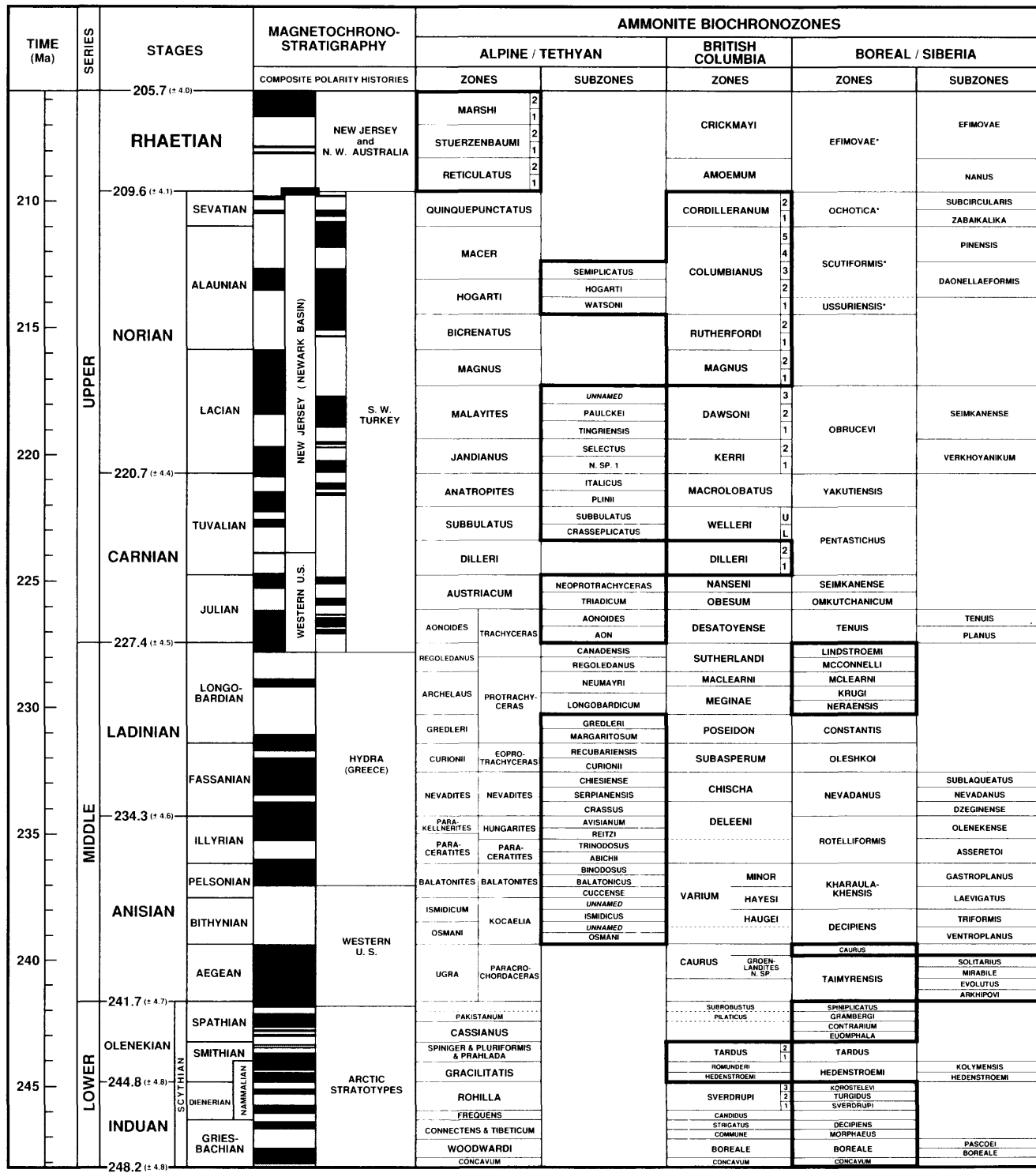


FIG. 8.—(E) Triassic magnetic polarity time scale comparison with highest-resolution ammonite subdivisions. The composite ammonite subdivision (heavy outline) is based on highest resolution information from Tethyan areas (De Zanche and others, 1993), British Columbia (L. Krystyn, as cited by Zapfe, 1993) and Boreal regions including Siberia. Ammonites are calibrated with standard stages and are assumed to have equal duration within each stage. The magnetic polarity history is calibrated with ammonite zones.

stratigraphic correlation of three independent studies (Horner, 1983; Galbrun and others, 1988; Galbrun and others, 1990).

Cretaceous Period

Cretaceous ammonite biostratigraphy in Europe is primarily based on Robaszynski and others (1980), Owen (1984, 1988), Hoedemaeker and Bulot (1990), Hancock (1991), Amédro (1992), Bulot and others (1993), Bulot and Thieuloy (1993), and Hoedemaeker and others (1993).

In the upper Cretaceous strata of Europe, high-resolution ammonite zonations exist for the Cenomanian through Santonian Stages, but the Campanian and Maastrichtian Stages are characterized by a much lower resolution ammonite biostratigraphy. In northern Europe, belemnites provide an alternative high-resolution subdivision for the Campanian through Maastrichtian Stages although prospects for correlation with this group appear limited. In North America, however, a high-resolution ammonite zonation (Cobban and others, 1994) is available for the Cenomanian through lower Maastrichtian interval. A significant number of ammonite zones in the Western Interior are radiometrically well dated (Obradovich, 1993), while the remainder of the zones are interpolated by assigning equal time to each zone (Fig. 8A). The Campanian/Maastrichtian boundary in Europe is between the *hyatti* and *neubergicus/tridens* ammonite Zones corresponds to the base of the *Belemnella lanceolata* Zone (Birkelund and others, 1984). This boundary is correlated to the base of the *Baculites eliasi* ammonite Zone (Kennedy and others, 1992) or slightly below (McArthur and others, 1993) in the Western Interior.

The lower Cretaceous time is subdivided into 66 ammonite zones and subzones (Fig. 8B). From the upper Valanginian to the Albian interval, zones/subzones were assigned equal duration in the absence of data. From the Berriasian through the lower Valanginian interval, ammonite zones were calibrated to some extent with paleomagnetic polarity information (Galbrun, 1984; Ogg and others, 1988; Ogg and others, 1991a).

TRIASSIC THROUGH CRETACEOUS SPLINES

Triassic and Early-Middle Jurassic Ages

In this section we discuss the final scaling of the Mesozoic ages. A secondary scaling is useful because, due to a general lack of radiometric dates, a drawback of the time scale constructed so far is that it is poorly defined for Early Triassic and Early and Middle Jurassic time.

PTS82 proposed the following method for dealing with segments of the geologic time scale where dates are scarce. Linear interpolation can be used to estimate the ages of stage boundaries between tie-points located near the beginning and the end of such a segment using the hypothesis of equal duration of stages between the tie-points. The tie-points themselves are stage boundaries with estimated ages that are relatively good. This method has the advantage of simplicity. However, it has a number of drawbacks: (1) certainty (zero standard deviation) is assigned to the tie-point estimates, and the estimates of uncertainty for all other stage boundaries are disregarded; (2) the length of duration of the stages, which is constant between tie-points, changes abruptly at the tie-points; and (3) it is more reasonable to assume equal duration of zones within stages.

PTS89 used equal duration of chronos in Mesozoic stages to further smooth chronogram age estimates for stage boundaries where chronos are units of equal duration within stages as derived from zones. The units were interpolated with "dog-legged" linear segments, showing abrupt changes at tiepoints, probably the result from hand fitting.

In this study, the equal duration of ammonite zones is used as a secondary scaling method to smooth Triassic and Jurassic stage boundary ages. These ages were scaled initially with maximum likelihood estimates. The approach, outlined below, uses a smoothing cubic spline where the uniform spacing of (sub)zones is the independent variable, and the irregularly spaced age estimates for stage boundaries from maximum likelihood (partly combined with direct estimates; Table 2, column 3) are the dependent variables. The approach is a statistical improvement on the maximum likelihood estimates and reduces uncertainty for stages with relatively large errors. For example, insufficient radiometric dates are available for the Induan, Olenekian, and Pliensbachian stages (Appendix 1), and errors are relatively large for Early and Middle Jurassic time. The effect of this scaling tool is directly proportional to the magnitude of the uncertainty, as outlined below. The tool has minimal effect on the duration of stages with small error bars.

The use of smoothing splines for interpolation over segments where dates are scarce is discussed by Agterberg (1988, 1990). A cubic spline function consists of a chain of cubic polynomials bounded by consecutive points (knots). The function represents the relation between a dependent variable (estimated ages of stage boundaries) and an independent variable (e.g., unequally spaced stage boundaries). The spline curve is smooth because it has continuous first and second derivatives (i.e., abrupt changes in slope and rate of change of slope are not permitted). It can be fitted by means of the least squares method. We used the algorithm originally developed by Reinsch (1967). This implies that the knots were selected at the observation points, the second derivative was set equal to zero at the first and last point, and the sum of squares of standardized residuals was set equal to the number of observations.

Two other properties of smoothing splines are as follows. Each observation is weighted according to the inverse of the square of its standard deviation. For the maximum likelihood estimates, the ratio of largest and smallest standard deviation exceeds 20. This means that the boundary with the smallest standard deviation (Permian/Triassic boundary with $\sigma = 0.28$, Table 2, column 3) will receive more than $400 \times$ as much weight as the boundary with the largest standard deviation (Carnian/Norian with $\sigma = 6.13$, Table 1, column 3). Another property is that, if all standard deviations are relatively large, the smoothing spline becomes a best-fitting straight line.

In total, 14 knots were used for the spline fitting. These are the 13 pre-Kimmeridgian stage boundaries with maximum likelihood estimates highlighted in Table 1 (see Table 2, column 3 for four revisions) plus the estimate for the Lower Pliensbachian Coldfish volcanics in British Columbia (Appendix 1, item 276). These knots were spaced such that distances between stratigraphic boundaries are proportional to the number of (sub)zones per stage; equal duration of ammonite zones was assumed within the Triassic and Jurassic separately. The knot for the Pliensbachian stage (Appendix 1, item 276) was spaced at one third of the total duration above the base of this stage.

In total, 17 ages were estimated by smoothing and interpolation with the cubic spline curve (Table 2, column 4). The final value is close to input if its standard deviation is small. The final value is primarily determined by the number of ammonite (sub)zones if its standard deviation is large or not used because of scarcity of dates.

Late Jurassic and Early Cretaceous Ages

Initially in this study, the Late Jurassic through Early Cretaceous stage boundaries were estimated by applying a variation of the method used to compute the earlier stage boundaries. The array of maximum likelihood estimates for these stage boundaries were combined with the independent estimates derived from the magnetochronology of a fixed spreading-rate for Hawaiian lineations. This merger of the two independent age estimates incorporated a weighted average based upon the relative standard deviations on each age. A cubic smoothing spline was passed through the array of merged stage boundary estimates using the uniform spacing of subzones as the independent variable. This statistical optimization of the radiometric, magnetic and biostratigraphic data yielded the following suite of age estimates:

Aptian/Albian	112.4 ± 0.9 (Ma \pm 2s)
Barremian/Aptian	120.5 ± 1.6
Hauterivian/Barremian	126.6 ± 1.8
Valanginian/Hauterivian	131.2 ± 1.7
Berriasian/Valanginian	135.7 ± 1.4
Tithonian/Berriasian	141.3 ± 1.9
Kimmeridgian/Tithonian	148.2 ± 1.9
Oxfordian/Kimmeridgian	153.3 ± 1.5
Callovian/Oxfordian	159.1 ± 1.6

The Kimmeridgian through Barremian Stage boundaries are systematically younger by approximately 0.5–1 my than the estimates derived entirely from the constant-spreading rate model for the Hawaiian magnetic lineation set. The main causes of this offset are (1) some relatively young ages reported for some of these stages and (2) the large number of ammonite subzones within the Kimmeridgian and Tithonian Stages within the Boreal realm as compared to Early Cretaceous stages (Appendix 1). The computed relative duration of stages, which is influenced by the relative number of ammonite subzones, would imply relatively faster Pacific spreading rates during the Oxfordian, Valanginian, and Barremian intervals, and relatively slower spreading rates during the Kimmeridgian-Berriasian and Hauterivian intervals. In contrast to the variable rates in the Pacific, this scale would imply that the Keathley sequence of the Central Atlantic was formed by a relatively smooth spreading rate. To a first approximation, these changes in Pacific spreading rates were suggested to be a factor in long-term changes in eustatic sea level.

However, Channell (this volume) further analyzed the implications of this initial scale ("GRAD93") and other time scales for spreading rates in different ocean basins and accumulation rates of pelagic sediments, and he concluded that the constant spreading-rate model for the Hawaiian magnetic lineation set is a preferable scale that does not cause artifacts of irregular spreading and accumulation rates. The constant-rate Hawaiian

scale is within the error limits of the maximum likelihood estimates from radiometric ages. Therefore, we have used a constant spreading rate for the Hawaiian lineations as the main control on derivation of stage boundaries within this interval and have not used the number of ammonite subzones for a secondary scaling factor. An implication is that the durations of ammonite subzones within the Boreal realm during the Kimmeridgian-Tithonian intervals were very brief (Fig. 8C).

Late Cretaceous Ages

As pointed out in the section on "Age Estimates for Selected Stratigraphic Boundaries," our best estimate for the age of the Maastrichtian-Danian (Cretaceous/Paleogene) boundary is 65.00 ± 0.04 Ma. This new estimate is significantly different from the maximum likelihood value of 66.06 ± 0.41 Ma (Table 1, column 2) which was rejected for that reason.

Obradovich (1993) directly interpolated the age of Late Cretaceous stage boundaries from over 30 closely spaced, $^{40}\text{Ar}/^{39}\text{Ar}$ radiometric estimates in United States Western Interior bentonites dated with ammonites (Table 3). All Ar/Ar age estimates were calibrated with 520 MMhb-1.

According to OB93, the age estimates for the stage boundaries are as follows: Campanian/Maastrichtian is 71.30 ± 0.25 Ma, Santonian/Campanian is 83.50 ± 0.25 Ma, Coniacian/Santonian is 86.30 ± 0.25 Ma, Turonian/Coniacian is 88.70 ± 0.25 Ma, Cenomanian/Turonian is 93.30 ± 0.10 , and Albian/Cenomanian is 98.50 ± 0.25 Ma.

We re-evaluated the local ammonite calibration in terms of European stage assignments and accepted the chronostratigraphy of OB93 accompanying the radiometric age estimates. Stratigraphic details on the relatively young Campanian/Maastrichtian boundary were discussed earlier. In this study, all $^{40}\text{Ar}/^{39}\text{Ar}$ age estimates were entered in Appendix 1.

TABLE 3.—U. S. WESTERN INTERIOR AMMONITE ZONES AND Ar/Ar DATES

Zone	$^{40}\text{Ar}/^{39}\text{Ar}$ Ages for Bentonites, Ma	Geologic Age
<i>Baculites clinolobatus</i>	69.42 ± 0.37	early Maastrichtian
<i>Baculites compressus</i>	73.35 ± 0.39	late Campanian
<i>Exteiloceras jenneyi</i>	74.76 ± 0.45	late Campanian
<i>Didymoceras stevensonii</i>	75.37 ± 0.39	late Campanian
<i>Didymoceras nebrascense</i>	75.89 ± 0.72	late Campanian
<i>Baculites obtusus</i>	80.54 ± 0.55	mid Campanian
<i>Scaphites hippocrepis II</i>	81.71 ± 0.34	early Campanian
<i>Desmocerasites bassleri</i>	83.91 ± 0.43	late Santonian
Just below <i>Boehmoceras assemblage</i>	84.09 ± 0.40	late Santonian
Top of <i>Inoceramus undulatoplicatus</i>		
Zone	84.88 ± 0.28	early Santonian
<i>Protexanites bourgeoisiensis</i>	86.92 ± 0.39	late Coniacian
<i>Scaphites preventricosus</i>	88.34 ± 0.60	mid Coniacian
<i>Prionoceras macombi</i>	90.21 ± 0.72	mid Turonian
<i>Prionoceras hyatti</i>	90.51 ± 0.45	mid Turonian
<i>Vascoceras birchbyi</i>	93.40 ± 0.63	early Turonian
<i>Pseudaspidoceras flexuosum</i>	93.25 ± 0.55	early Turonian
<i>Neocardioceras judii</i>	93.30 ± 0.40	late Cenomanian
<i>N. judii</i>	93.78 ± 0.49	late Cenomanian
<i>N. judii</i>	93.59 ± 0.58	late Cenomanian
<i>Euomphaloceras septemseriatum</i>	93.49 ± 0.89	late Cenomanian
<i>Vascoceras diartianum</i>	93.90 ± 0.72	late Cenomanian
<i>Dunveganoceras pondi</i>	94.63 ± 0.61	late Cenomanian
<i>Acanthoceras amphibolium</i>	94.93 ± 0.53	mid Cenomanian
<i>Conlinoceras giberti</i>	95.78 ± 0.61	mid Cenomanian
27 m below <i>C. giberti</i>	95.86 ± 0.45	mid Cenomanian
<i>Neogastropites cornutus</i>	98.52 ± 0.41	early Cenomanian
<i>N. haasi</i>	98.54 ± 0.70	early Cenomanian

A cubic spline curve was fitted to the first 25 Ar/Ar dates of Table 3 for 6 stages (Cenomanian through Maastrichtian; Fig. 7). The relative positions of the 23 biozones associated with these bentonites were used for location in the curve-fitting exercise. These 23 biozones belong to a continuous sequence of 65 biozones extending from the base of the mid-Cenomanian to the middle of the early Maastrichtian. This interpolation gave precise results because the standard deviations of the 25 dates are relatively small, ranging from 0.14 to 0.45 Ma, and the observations fall nearly on a continuous curve. This interpolation is more accurate than the dog-legged (?hand-fitted) interpolation lines through the age estimated used in OB93. The following values were obtained by a method similar to the one explained earlier when discussing Triassic through Middle Jurassic spline smoothing:

Campanian/Maastrichtian	71.29 ± 0.25 Ma
Santonian/Campanian	83.46 ± 0.24 Ma
Coniacian/Santonian	85.79 ± 0.23 Ma
Turonian/Coniacian	88.96 ± 0.25 Ma
Cenomanian/Turonian	93.49 ± 0.08 Ma

Pre-Cenomanian Standard Deviations

Final standard deviations for the boundary ages older than Cenomanian were determined by fitting a separate spline-curve with input and output for the dependent variable as shown in Table 2, column 4. The final ages were used for the independent variable, and the degree of smoothing was determined by assigning equal weights to the input values, followed by cross-validation (Agterberg, 1990). Input values for the standard deviations of the Triassic stage boundaries were based on the parabola peaks (Table 1, column 1), because Triassic likelihood functions have relatively flat tops. Uncertainty of the final ages is expressed by means of 2σ precision (Table 2, column 5). It is not possible to estimate standard deviations for the durations because of lack of information on serial correlation of the stage boundary age estimates.

THE MESOZOIC TIME SCALE

The age estimates for the 30 stage boundaries (in Ma units $\pm 2\sigma$) are tabulated in the last column of Table 1 and in Table 4. Final age estimates were rounded to one decimal position and standard deviations are expressed at 2σ precision, which approximates the 95% confidence level. The uncertainty in the relative duration of each individual stage is much less than indicated by the uncertainties on the ages of the boundaries.

The ages of period boundaries are (in Ma $\pm 2\sigma$):

Permian/Triassic	248.2 ± 4.8 Ma
Triassic/Jurassic	205.7 ± 4.0
Jurassic/Cretaceous	144.2 ± 2.6
Cretaceous/Paleogene	65.0 ± 0.1 Ma

The boundary of the Induan and Olenekian stages of the Early Triassic is assigned solely according to the relative numbers of ammonite zonal units, 9 vs. 8 respectively. Radiometric age estimates are needed to corroborate and refine this age. The five longest stages are Norian at 11.1 my, Toarcian at 9.5 my, Aptian at 8.8 my, Albian at 13.3 my, and Campanian at 12.2

TABLE 4.—MESOZOIC TIME SCALE

Stage Boundary	Age, Ma	Duration of Preceding Stage, my
Maastrichtian/Danian (Cretaceous/Tertiary)	65.0 ± 0.1	6.3
Campanian/Maastrichtian	71.3 ± 0.5	12.2
Santonian/Campanian	83.5 ± 0.5	2.3
Coniacian/Santonian	85.8 ± 0.5	3.2
Turonian/Coniacian	89.0 ± 0.5	4.5
Cenomanian/Turonian	93.5 ± 0.2	5.4
Albian/Cenomanian	98.9 ± 0.61	3.3
Aptian/Albian	112.2 ± 1.1	8.8
Barremian/Aptian	121.0 ± 1.4	6.0
Hauterivian/Barremian	127.0 ± 1.6	5.0
Valanginian/Hauterivian	132.0 ± 1.9	5.0
Berriasian/Valanginian	137.0 ± 2.2	7.2
Tithonian/Berriasian (Jurassic/Cretaceous)	144.2 ± 2.6	6.5
Kimmeridgian/Tithonian	150.7 ± 3.0	3.4
Oxfordian/Kimmeridgian	154.1 ± 3.3	5.3
Callovian/Oxfordian	159.4 ± 3.6	5.0
Bathonian/Callovian	164.4 ± 3.8	4.8
Bajocian/Bathonian	169.2 ± 4.0	7.3
Aalenian/Bajocian	176.5 ± 4.0	3.6
Toarcian/Aalenian	180.1 ± 4.0	9.5
Pliensbachian/Toarcian	189.6 ± 4.0	5.7
Sinemurian/Pliensbachian	195.3 ± 3.9	6.6
Hettangian/Sinemurian	201.9 ± 3.9	3.8
Rhaetian/Hettangian (Triassic/Jurassic)	205.7 ± 4.0	3.9
Norian/Rhaetian	209.6 ± 4.11	1.1
Carnian/Norian	220.7 ± 4.4	6.7
Ladinian/Carnian	227.4 ± 4.5	6.9
Anisian/Ladinian	234.3 ± 4.6	7.4
Olenekian/Anisian	241.7 ± 4.7	3.1
Induan/Olenekian	244.8 ± 4.8	3.4
Tatarian/Induan (Permian/Triassic)	248.2 ± 4.8	

Uncertainty on ages of stage boundaries is given to 2 standard deviations.

my. Most stages are 5–6 my in duration. The Santonian is the shortest stage at 2.3 my.

The Mesozoic magnetic polarity reversals compiled by Ogg (1995) are displayed along the geologic time scale in Figures 8A–E. There are no magnetic anomalies preserved prior to the Callovian stage, and the pre-Oxfordian polarity time scale is tentative pending further verification in multiple fossiliferous sedimentary section.

When using the estimates of uncertainty, no simple solution exists for combining stratigraphic uncertainty of relative age data with analytical uncertainty of radiometric age estimates in a single statistical number. In this study, two approaches are combined in time scale calculation:

1. Stratigraphic interpolation of analytically precise age estimates close to key stage boundaries, and
2. Stratigraphic/statistical analysis with maximum likelihood estimation and spline smoothing of numerous, stratigraphically meaningful radiometric age estimates.

The second approach allows estimation of error bars. In order to further reduce uncertainty levels, more radiometric dates are needed in pre-Aptian marine strata, with particular emphasis on the Jurassic Period.

The advent of radiometric dating techniques with less than 1% analytical error, as demonstrated in the new Cretaceous Ar/Ar dates, furnishes a major challenge to biostratigraphy. It used to be that biostratigraphic resolution in the Mesozoic Era largely surpassed that based on radiometric dates, but the gap is closing. Even the most detailed biostratigraphic scheme probably has no biozonal units of less than 0.5–1.0 my duration, not to speak

of the actual precision in dating a particular "piercing point" for which an Ar/Ar age estimate would be available with an analytical uncertainty of 0.1 to 0.5 my. The combination of such dates with high-resolution biostratigraphy, magnetostratigraphy, or Milankovitch cyclicity is a major challenge for Mesozoic geochronologic studies.

SUMMARY AND CONCLUSIONS

In this study, we derive an absolute geologic time scale, integrated with ammonite zones and magnetic polarity chronos for the Triassic, Jurassic and Cretaceous Periods, together comprising the Mesozoic Era. The geologic time scale is composed of standard stratigraphic units (stages), calibrated in millions of years, with an uncertainty estimate at each level (Fig. 9). Stratigraphically critical data, underpinning this isotopic age dates framework, incorporate the observed ties between (1) radiometric dates, biozones and stage boundaries, and (2) biozones and magnetic reversals on the seafloor and in sediments.

One reason to propose the new time scale for the Mesozoic is that over 65 new Triassic, Jurassic and Cretaceous age dates have become available since 1989 (an increase of 25% since PTS89). Also, improvements in calibrations of stages, standard

zones, and magnetic polarity reversals, and development of better interpolation techniques where age control is sparse, enable updating previously proposed age estimates for the stage boundaries in the Triassic, Jurassic and Cretaceous Periods. We have preserved estimates of uncertainty for the age of each stage boundary. The uncertainty in relative duration of each individual stage is much less than the uncertainties on the ages of the stage boundaries. It is not possible to estimate standard deviations for the durations because of lack of information on serial correlation of the stage boundary age estimates. As shown in the last column of Table 1, the ratio of stage duration estimates for the Mesozoic time scale fluctuates between 0.2 and 1.7. The stage duration estimates are relatively precise. Nevertheless, the large differences between results based on successive time scales, (Figs. 1–3) suggest that the Mesozoic time scale needs further improvement, especially the Jurassic and Lower Cretaceous parts.

The ages of period boundaries are (in Ma \pm 2s): Permian/Triassic = 248.2 ± 4.8 Ma, Triassic/Jurassic = 205.7 ± 4.0 Ma, Jurassic/Cretaceous = 144.2 ± 2.6 Ma, and Cretaceous/Paleogene = 65.0 ± 0.1 Ma.

Note.—In June 1995, Brack et al. reported single-grain zircon U/Pb age dates from tuffaceous layers associated with the Anisian/Ladinian boundary interval in sections near Bagolino in northern Italy. This region is a proposed candidate for the Global Stratotype Section and Point of the base of the Ladinian stage, although disagreements on the precise level have not yet been resolved. A suite of seven zircons from a thin crystal tuff in the lower part of the *Secedensis [Nevadites]* ammonite zone yielded a weighted Pb/U mean age of 241.0 ± 0.5 Ma. This same bed can be traced to equivalent tuffs in the Grenzbitumenzone at Monte San Giorgio in southern Switzerland (Brack and Rieber, 1993). As summarized in our text, sanidine feldspars from these tuffs in the Grenzbitumenzon had previously yielded a mean K/Ar age of 233 ± 4.5 Ma (2s) and a plateau age of approximately 232 ± 4.5 Ma (2s) (Hellmann and Lippolt, 1981; discussed as NDS196 in Odin, 1982; incorporated as items 309 and 310 in Appendix), which were key age controls on the final computed age of 234.3 ± 4.6 Ma for this stage boundary. However, Brack et al. (1995) report that preliminary zircon ages from this same Grenzbitumenzone are consistent with their age from Bagolino.

Incorporation of the new radiometric date for this boundary interval and other zircon ages (Brack et al., 1995) for overlying middle Ladinian tuffs (238.8 ± 0.4 Ma in the middle of Gredleri Zone; 237.7 ± 0.5 Ma in the middle of Archelaus Zone) into the maximum-likelihood database and new spline computations imply a longer time span for the Ladinian Stage (8.3 instead of 6.9 my), and a greatly reduced extent of the Anisian Stage (3.1 instead of 7.4 my). However, Brack et al. (1995) recommend placement of the *Nevadites* Zone into the Anisian Stage, rather than its traditional placement in the Ladinian, which would result in a younger Anisian/Ladinian boundary.

ACKNOWLEDGMENTS

The following colleagues provided valuable criticism and advice on data and methods adopted in this study or supplied new stratigraphic information: Sven Backstrom, William Berggren, Timothy Bralower, James Channell, Elisabetta Erba, Martin Farley, Jason Hicks, Ph. Hoedemaker, Thierry Jacquin, Dennis

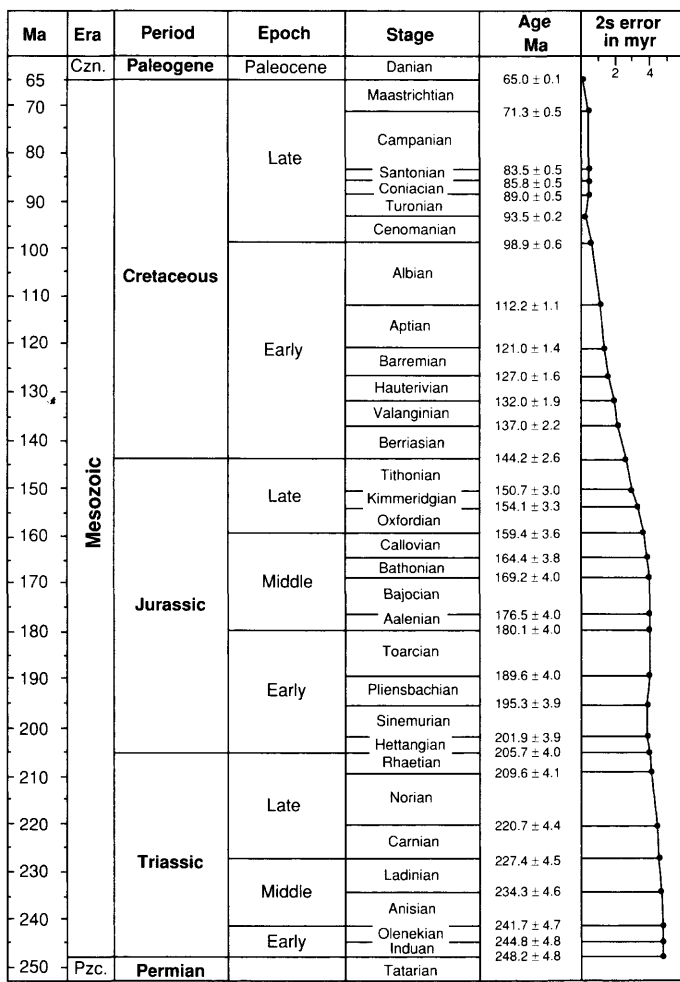


FIG. 9.—The Mesozoic geologic time scale.

Kent, Han Leerveld, Ian Lerche, J.M. McArthur, Peter McLaughlin, J. Mortensen, Giovanni Muttoni, John Obradovich, Neil Opdyke, Serge Odin, Katherina Perch-Nielsen, Malcolm Pringle, Will Sager, P. Smith, Henk Visscher, and Gerd Westermann. We thank Exxon Production Research Company for supporting this project. Portions of the text and figures from "A Mesozoic time scale" by Gradstein and others (1994) are used by permission of the American Geophysical Union.

REFERENCES

- AGTERBERG, F. P., 1988, Quality of time scales: a statistical appraisal, in Merriam, D. F., ed., *Current Trends in Geomathematics*: New York, Plenum, p. 57–103.
- AGTERBERG, F. P., 1990, *Automated Stratigraphic Correlation*: New York, Elsevier, 424 p.
- ALVAREZ, W., ARTHUR, M. A., FISCHER, A. G., LOWRIE, W., NAPOLEONE, G., PREMOLI-SILVA, I., AND ROGGERENTH, W. M., 1977, Upper Cretaceous-Paleocene magnetic stratigraphy at Gubbio, Italy. V. Type section for the Late Cretaceous-Paleocene geomagnetic reversal time scale: *Bulletin of the Geological Society of America*, v. 88, p. 383–389.
- AMÉDRO, F., 1992, L'Albian du Bassin Anglo-Parisiens: Ammonites, zonation phyletic, sequences: *Bulletin des Centres de Recherches Exploration-Production Elf-Aquitaine*, v. 16, p. 187–233.
- ARMSTRONG, R. L., 1978, Pre-Cenozoic Phanerozoic time scale: Computer file of critical dates and consequences of new and in-progress decay-constant revisions, in Cohee, G. V., Glaessner, M. F., and Hedberg, H. D., eds., *The Geologic Time Scale*: Tulsa, American Association of Petroleum Geologists, *Studies in Geology* 6, p. 73–91.
- BERGGREN, W. A., KENT, D. V., OBRADOVICH, J. D., AND SWISHER, III, C. C., 1992, Towards a revised Paleogene geochronology, in Prothero, D. R. and Berggren, W. A., eds., *Eocene-Oligocene Climatic and Biotic Evolution*: Princeton, Princeton University Press, p. 29–45.
- BIRKELUND, T., HANCOCK, J. M., HART, M. B., RAWSON, P. F., REMANE, J., ROBASZYNSKI, F., SCHMID, F., AND SURLYK, F., 1984, Cretaceous stage boundaries: proposals: *Bulletin of the Geological Society of Denmark*, v. 33, p. 3–20.
- BOLES, J. R. AND LANDIS, C. A., 1984, Jurassic sedimentary melange and associated facies, Baja California, Mexico: *Geological Society of American Bulletin*, v. 95, p. 513–521.
- BRACK, P. AND RIEBER, H., 1993, Towards a better definition of the Anisian/Ladinian boundary: New biostratigraphic data and correlations of boundary sections from the Southern Alps: *Eclogae Geologicae Helvetiae*, v. 86, p. 415–427.
- BRACK, P., RIEBER, H., AND MUNDI, R., 1995, The Anisian/Ladinian boundary interval at Bagolino (southern Alps, Italy): I. Summary and new results on ammonoid horizons and radiometric age dating: *Albertiana* 15: 45–56.
- BRALOWER, T. J., LUDWIG, K. R., OBRADOVICH, J. D., AND JONES, D. L., 1990, Berriasian (Early Cretaceous) radiometric ages from the Grindstone Creek Section, Sacramento Valley, California: *Earth and Planetary Science Letters*, v. 98, p. 62–73.
- BRALOWER, T. J., THIERSTEIN, H. R., AND MONECHI, S., 1989, Calcareous nannofossil zonation of the Jurassic-Cretaceous boundary interval and correlation with the geomagnetic polarity time scale: *Marine Micropaleontology*, v. 14, p. 153–235.
- BUCHER, H., 1989, Lower Anisian ammonoids from the northern Humbolt Range (northwest Nevada, USA) and their bearing upon the Lower-Middle Triassic boundary: *Eclogae Geologicae Helvetiae*, v. 82, p. 945–1002.
- BULOT, L., BLANC, E., THIEULOUY, J. P., AND REMANE, J., 1993, La limite Berriasien-Valanginién dans le Sud-Est de la France: données biostratigraphiques nouvelles: *Comptes Rendus de l'Academie des Sciences, Série 2, Mécanique, Physique, Chimie, Sciences de l'Univers, Sciences de la Terre*, v. 316, p. 1771–1778.
- BULOT, L., AND THIEULOUY, J. P., 1993, Implications chronostratigraphiques de la révision de l'échelle biostratigraphique du Valanginién supérieur et de l'Hauterivien du Sud-Est de la France: *Comptes Rendus de l'Academie des Sciences, Série 2, Mécanique, Physique, Chimie, Sciences de l'Univers, Sciences de la Terre*, v. 317, p. 387–394.
- CANDE, S. C. AND KENT, D. V., 1992, A new geomagnetic polarity time scale for the Late Cretaceous and Cenozoic: *Journal of Geophysical Research*, v. 97, p. 13917–13951.
- CANDE, S. C., LARSON, R. L., AND LABRECQUE, J. L., 1978, Magnetic lineations in the Pacific Jurassic Quiet Zone: *Earth and Planetary Science Letters*, v. 41, p. 434–440.
- CECCA, F., PALINI, G., ERBA, E., PREMOLI-SILVA, I., AND COCCIONI, R., 1994, Hauterivian-Barremian chronostratigraphy based on ammonites, nannofossils, planktonic foraminifera, and magnetic chronos from the Mediterranean domain: *Cretaceous Research*, v. 15, p. 457–467.
- CHANNELL, J. E. T. AND ERBA, E., 1992, Early Cretaceous polarity chronos CM0 to CM11 recorded in northern Italian land sections near Brescia: *Earth and Planetary Science Letters*, v. 108, p. 161–179.
- CHANNELL, J. E. T., MASSARI, F., BENETTI, A., AND PEZZONI, N., 1990, Magnetoostratigraphy and biostratigraphy of Callovian-Oxfordian limestones from the Trento Plateau (Monti Lessini, northern Italy): *Palaeogeography, Palaeoclimatology, Palaeoecology*, v. 79, p. 289–303.
- CLAQUE-LONG, J. C., ZICHAO, Z., GUOGAN, M., AND SHAOHUA, D., 1991, The age of the Permian-Triassic boundary: *Earth and Planetary Science Letters*, v. 105, p. 182–190.
- COBBAN, W. A., MEREWETHER, E. A., FOUCHE, T. D., AND OBRADOVICH, J. D., 1994, Some Cretaceous shorelines in the Western Interior of the United States, in Caputo, M. V., Peterson, J. A., and Franczyk, K. J., eds., *Mesozoic Systems of the Rocky Mountain Region*, USA: p. 393–425.
- COPE, J. C. W., GETTY, T. A., HOWARTH, M. K., MORTON, N., AND TORRENS, T. S., 1980a, A correlation of Jurassic rocks in the British Isles. Part One: Introduction and Lower Jurassic: Oxford, Geological Society of London Special Report 14, 73 p.
- COPE, J. C. W., DUFF, K. L., PARSONS, C. F., TORRENS, T. S., WIMBLEDON, W. A., AND WRIGHT, J. K., 1980b, A correlation of Jurassic rocks in the British Isles. Part Two: Middle and Upper Jurassic: Oxford, Geological Society of London Special Report 15, 109 p.
- CORNEL, B. AND OLSEN, P. E., 1985, A summary of the biostratigraphy of the Newark Supergroup of Eastern North America, in Weber, R., ed., *III Congreso Latinoamericano de Paleontología, Mexico, Simposia Floras del Triásico Tardío, su Fitogeografía y Paleoecología, Memoria*: Mexico City, Universidad Nacional Autónoma de Mexico, Instituto de Geología, p. 67–81.
- COWIE, J. W. AND BASSETT, M. G., 1989, 1989 Global Stratigraphic Chart: Ottawa, International Union of Geological Sciences.
- COX, A. V. AND DALRYMPLE, G. B., 1967, Statistical analysis of geomagnetic reversal data and the precision of potassium-argon dating: *Journal of Geophysical Research*, v. 72, p. 2603–2614.
- DAGYS, A. S., 1988, Boundary of the Lower and Middle Triassic in Boreal and Tethyan regions and correlation of Anisian deposits: *Geologiya i Geofizika*, v. 29, p. 3–9.
- DAGYS, A. S. AND KONSTANTINOV, A. G., 1992, A new zonal scheme of the boreal Ladinian: *Albertiana*, v. 10, p. 17–21.
- DAGYS, A. S. AND WEITSCHAT, W., 1993, Correlation of the Boreal Triassic: *Mitteilungen aus dem Geologisch Paläontologischen Institut der Universität Hamburg*, v. 75, p. 249–256.
- DAGYS, A. S., WEITSCHAT, W., KONSTANTINOV, A., AND SOBOLEV, E., 1993, Evolution of the boreal marine biota and biostratigraphy at the Middle/Upper Triassic boundary: *Mitteilungen aus dem Geologisch Paläontologischen Institut der Universität Hamburg*, v. 75, p. 193–209.
- DE ZANCHE, V., GIANOLLA, P., MIETTO, P., SIORPAES, C., AND VAIL, P., 1993, Triassic sequence stratigraphy in the Dolomites (Italy): *Memorie di Scienze Geologiche*, v. 45, p. 1–27.
- DEMING, W. E., 1948, *Statistical Adjustment of Data*: New York, Wiley, 261 p.
- FOLAND, K. A., GILBERT, L. A., SEBRING, C. A., AND JIANG-FENG, C., 1986, $^{40}\text{Ar}/^{39}\text{Ar}$ ages for plutons of the Monteregian Hills, Quebec: Evidence for a single episode of Cretaceous magmatism: *Bulletin of the Geological Society of America*, v. 97, p. 966–974.
- FORSTER, S. C. AND WARRINGTON, G., 1985, Geochronology of the Carboniferous, Permian and Triassic, in Snelling, N. J., ed., *The Chronology of the Geological Record*: Oxford, Blackwell Scientific Publishers, Geological Society of London Memoir 10, p. 99–113.
- FOWELL, S. J. AND OLSEN, P. E., 1993, Time calibration of Triassic/Jurassic microfloral turnover, eastern North America: *Tectonophysics*, v. 222, p. 361–369.
- GAETANI, M., 1992, Report on the Symposium on Triassic Stratigraphy (Lausanne, October 20–23, 1991): *Albertiana*, v. 10, p. 6–9.
- GAETANI, M. (ed.), 1993a, I.U.G.S. Subcommission on Triassic Stratigraphy, Anisian/Ladinian boundary field workshop, Southern Alps-Balaton Highlands, 27 June–4 July 1993: Milano, Dipartimento di Scienze della Terra, Università degli Studi, 117 p.

- GAETANI, M., 1993b, Anisian/Ladinian Boundary Field Workshop, Report: Albertiana, v. 12, p. 5–9.
- GALBRUN, B., 1984, Magnétostratigraphie de la limite Jurassique-Créacé. Proposition d'une échelle de polarité à partir du stratotype du Berriasien (Berrias, Ardèche, France) et la Sierra de Lugar (Province de Murcie, Espagne): Paris, Mémoires des Sciences de la Terre, Univ. Pierre et Marie Curie, 95 p.
- GALBRUN, B., BAUDIN, F., FOURCADE, E., AND RIVAS, P., 1990, Magnetostratigraphy of the Toarcian Ammonitico Rosso limestone at Iznalloz, Spain: Geophysical Research Letters, v. 17, p. 2441–2444.
- GALBRUN, B., GABILLY, J., AND RASPLUS, L., 1988, Magnetostratigraphy of the Toarcian stratotype sections at Thouars and Airvault (Deux-Sèvres, France): Earth and Planetary Science Letters, v. 87, p. 453–462.
- GALLET, Y., BESSE, J., KRYSYNT, L., MARCOUX, J., AND THÉVENIAUT, H., 1992, Magnetostratigraphy of the Late Triassic Bolüecktasi Tepe section (southwestern Turkey): implications for changes in magnetic reversal frequency: Physics of the Earth and Planetary Interiors, v. 73, p. 85–108.
- GALLET, Y., BESSE, J., KRYSYNT, L., THÉVENIAUT, H., AND MARCOUX, J., 1993, Magnetostratigraphy of the Kavur Tepe section (southwestern Turkey): A magnetic polarity time scale for the Norian: Earth and Planetary Science Letters, v. 117, p. 443–456.
- GRADSTEIN, F. M., AGTERBERG, F. P., AUBRY, M.-P., BERGGREN, W. A., FLYNN, J. J., HEWITT, R., KENT, D. V., KLITGORD, K. D., MILLER, K. G., OBRADOVICH, J. D., OGG, J. G., PROTHERO, D. R., AND WESTERMANN, G. E. G., 1988, Sea level history: Science, v. 214, p. 599–601.
- GRADSTEIN, F. M., AGTERBERG, F. P., OGG, J. G., HARDENBOL, J., VAN VEEN, P., THIERRY, J., AND HUANG, Z., 1994, A Mesozoic time scale: Journal of Geophysical Research, v. 99, p. 24051–24074.
- GROUPE FRANÇAIS D'ÉTUDES DU JURASSIQUE, 1991, Réactualisation des zones d'ammonites, in 3rd International Symposium on Jurassic Stratigraphy: Poitiers, International Subcommission of Jurassic Stratigraphy, Lyon, France, abstract volume, p. 124–134.
- HALLAM, A. J. M., HANCOCK, J. M., LABREQUE, J. L., LOWRIE, W., AND CHANNELL, J. E. T., 1985, Jurassic and Cretaceous geochronology and Jurassic to Paleogene magnetostratigraphy, in Snelling, N. J., ed., The Chronology of the Geological Record: Oxford, Blackwell Scientific Publishers, Geological Society of London Memoir 10, p. 118–140.
- HANCOCK, J. M., 1991, Ammonite scales for the Cretaceous System: Cretaceous Research, v. 12, p. 259–291.
- HANDSCHUMACHER, D. W., SAGER, W. W., HILDE, T. W. C., AND BRACEY, D. R., 1988, Pre-Cretaceous evolution of the Pacific plate and extension of the geomagnetic polarity reversal time scale with implications for the origin of the Jurassic “Quiet Zone”: Tectonophysics, v. 155, p. 365–380.
- HAQ, B. U., HARDENBOL, J., AND VAIL, P. R., 1988, Mesozoic and Cenozoic chronostratigraphy and cycles of sea-level change, in Wilgus, C. K., Hastings, B. S., Ross, C. A., Posamentier, H. W., Van Wagoner, J., and Kendall, G. St. C., eds., Sea-Level Changes: An Integrated Approach: Tulsa, Society of Economic Paleontologists and Mineralogists Special Publication 42, p. 71–108.
- HARLAND, W. B., COX, A. V., LLEWELLYN, P. G., PICKTON, C. A. G., SMITH, A. G., AND WALTERS, R., 1982, A Geologic Time Scale: Cambridge, Cambridge University Press, 131 p.
- HARLAND, W. B., ARMSTRONG, R. L., COX, A. V., CRAIG, L. E., SMITH, A. G., AND SMITH, D. G., 1990, A Geologic Time Scale 1989: Cambridge, Cambridge University Press, 265 p.
- HARPER, G. D., 1984, The Josephine ophiolite, northwestern California: Bulletin of the Geological Society of America, v. 95, p. 1009–1026.
- HELLMANN, K. N. AND LIPPOLT, H. J., 1981, Calibration of the Middle Triassic time scale by conventional K-Ar and Ar-Ar dating of alkali feldspars: Journal of Geophysics, v. 50, p. 73–86.
- HERBERT, T. D., 1992, Paleomagnetic calibration of Milankovitch cyclicity in Lower Cretaceous sediments: Earth and Planetary Science Letters, v. 112, p. 15–28.
- HICKS, J. F., 1993, Chronostratigraphic analysis of the foreland basin sediments of the latest Cretaceous, Wyoming, U.S.A.: Unpublished Ph.D. Dissertation, Yale University, New Haven, 250 p.
- HODYCH, J. P. AND DUNNING, G. R., 1992, Did the Manicouagan impact trigger end-of-Triassic mass extinction?: Geology, v. 20, p. 51–54.
- HORNER, F., 1993, Palaeomagnetismus von Karbonatsedimenten der Südlichen Tethys: Implikationen für die Polarität des Erdmagnetfeldes im untern Jura und für die tektonik der Ionischen zone Grieschenlands: Unpublished Ph.D. Dissertation, ETH Zürich, 139 p.
- HOEDEMAEKER, PH. J. AND BULOT, L., 1990, Preliminary ammonite zonation of the Lower Cretaceous of the Mediterranean region: Géologie Alpine, v. 66, p. 123–127.
- HOEDEMAEKER, PH. J., COMPANY, M., AGUIRRE-URRETTA, B., AVRAME, BOGDANOVA, T. N., BULOT, L., CECCA, F., DELANNOY, G., ETTACHFINI, M., MEMMIL, OWEN, H. G., RAWSON, A. F., SANDOVAL, J., TAVERA, J. M., THIEULOUY, J. P., TOVBINA, S. Z., AND VASICEK, Z., 1993, Ammonite zonation for the Lower Cretaceous of the Mediterranean region, basis for stratigraphic correlations within IGCP Project 262: Revista Española Paleontología, v. 8, p. 117–120.
- HOLSER, W. T. AND MAGARITZ, M., 1987, Events near the Permian-Triassic boundary: Modern Geology, v. 11, p. 155–180.
- HOLSER, W. T., SCHÖNLÄUB, H.-P., BOECKELMANN, K., AND MAGARITZ, M., 1991, The Permian-Triassic of the Gartnerfokel-1 Core (Carnic Alps, Austria): synthesis and conclusions: Abhandlungen der Geologischen Bundesanstalt, v. 45, p. 213–232.
- KAZAKOV, A. M. AND KURUSHIN, N. I., 1992, Stratigraphy of Norian and Rhaetian deposits in the northern middle Siberia: Russian Geology and Geophysics, v. 33, p. 1–8.
- KENNEDY, W. J., COBBAN, W. A., AND SCOTT, G. R., 1992, Ammonite correlation of the uppermost Campanian of Western Europe, the U.S. Gulf Coast, Atlantic Seaboard and Western Interior, and the numerical age of the base of the Maastrichtian: Geological Magazine, v. 129, p. 497–500.
- KENT, D. V. AND GRADSTEIN, F. M., 1985, A Cretaceous and Jurassic chronology: Bulletin of the Geological Society of America, v. 96, p. 1419–1427.
- KENT, D. V. AND GRADSTEIN, F. M., 1986, A Jurassic to Recent chronology, in Vogt, P. R. and Tucholke, B. E., eds., The Western North Atlantic Region: Boulder, Geological Society of America, The Geology of North America, Volume M, p. 45–50.
- LARSON, R. L. AND HILDE, T. W. C., 1975, A revised time scale of magnetic reversals for the Early Cretaceous and Late Jurassic: Journal of Geophysical Research, v. 80, p. 2586–2594.
- LARSON, R. L., LANCELOT, Y., AND OTHERS, 1992, Proceedings of the Ocean Drilling Program, Scientific Results, v. 129: College Station, Ocean Drilling Program, 745 p.
- LUDDEN, J., 1992, Radiometric age determinations for basement from Sites 765 and 766, Argo Abyssal Plain and Northwestern Australia: Proceedings of the Ocean Drilling Program, Scientific Results, v. 123, p. 557–559.
- MARCOUX, J., 1993, Comparison between the magnetostratigraphic sequences obtained from Bolüecktasi Tepe and the Kavur Tepe sections (southwestern Turkey): Albertiana, v. 12, p. 67.
- MARCOUX, J., GIRARDEAU, J., FOURCADE, E., BASSOULET, J. P., PHILIP, J., JAFFREZO, M., XUCHANG, X., AND CHENGFA, C., 1987, Geology and biostratigraphy of the Jurassic and lower Cretaceous series to the north of the Lhasa Block (Tibet, China): Geodinamica Acta, v. 1, p. 313–325.
- MICARTHUR, J. M., THIRWALL, M. F., CHEN, M., GALE, A. S., AND KENNEDY, W. J., 1993, Strontium isotope stratigraphy in the Late Cretaceous: Numerical calibration of the Sr isotope curve and intercontinental correlation for the Campanian: Paleoceanography, v. 8, p. 859–873.
- MESZEZHNIKOV, M. S., 1988, Tithonian (Volgian), in Krymholtz, G. Ya., Meszhnikov, M. S., and Westermann, G. E. G., eds., The Jurassic Ammonite Zones of the Soviet Union: Boulder, Geological Society of America Special Paper 223, p. 50–62.
- MORBAY, S. J., 1978, Late Triassic and Early Jurassic subsurface palynostratigraphy in northwestern Europe, in Cramer, F. H., Diez, M. D. C. R., and Gutierrez, M., eds., First International Palynological Conference, Palinologia, extraordinaria 1, p. 355–366.
- MOSTLER, H., SCHEURING, B., AND URLICH, M., 1978, Zur Mega-, Mikrofauna und Mikroflora der Koessener Schichten (alpine Obertrias) vom Weisloferbach in Tirol unter besonderer Berücksichtigung der in der suessi- und marshi-Zone auftretenden Conodonten: Schriftenreihe der Erdwissenschaftlichen Kommissionen, Österreichische Akademie der Wissenschaften, v. 4, p. 141–171.
- MUTTONI, G., CHANNELL, J. E. T., NICORA, A., AND RETTORI, R., 1994, Magnetostratigraphy and biostratigraphy of an Anisian-Ladinian (Middle Triassic) boundary section from Hydra (Greece): Palaeogeography, Palaeoclimatology, Palaeoecology, v. 111, p. 249–262.
- NAKAZAWA, K., 1992, The Permian-Triassic boundary: Albertiana, v. 10, p. 23–30.
- NALIVKIN, D. V. (N. Rast, translator), 1973, in Geology of the USSR: Edinburgh, Oliver and Boyd, 855 p.
- OBRADOVICH, J. D., 1988, A different perspective on glauconite as a chronometer for geologic time scale studies: Paleoceanography, v. 3, p. 757–770.

- OBRADOVICH, J. D., 1993, A Cretaceous time scale, in Caldwell, W. G. E., ed., Evolution of the Western Interior Basin: Ottawa, Geological Association of Canada Special Paper 39, p. 379–396.
- ODIN, G. S. (ed.), 1982, Numerical Dating in Stratigraphy, Pt. 1 and 2: Chichester, J. Wiley and Sons, 1040 p.
- ODIN, G. S. (ed.), 1992a, Phanerozoic Time Scale: Paris, Bulletin de Liason and Informations, IUGS Subcommission on Geochronology, v. 9.
- ODIN, G. S. (ed.), 1992b, Phanerozoic Time Scale: Paris, Bulletin de Liason and Informations, IUGS Subcommission on Geochronology, v. 10, p. 1–56.
- ODIN, G. S. AND ODIN, C., 1990, Echelle Numérique des Temps Géologiques: Geochronologie, v. 35, p. 12–20.
- OGG, J. G., 1988, Early Cretaceous and Tithonian magnetostratigraphy of the Galicia margin (Ocean Drilling Program Leg 103): College Station, Proceedings of the Ocean Drilling Program, Scientific Results, v. 103, p. 659–681.
- OGG, J. G., 1995, Magnetic polarity time scale of the Phanerozoic, in Ahrens, T., ed., Global Earth Physics: A Handbook of Physical Constants: Washington, American Geophysical Union Reference Shelf, v. 1, p. 240–270.
- OGG, J. G., COMPANY, M., STEINER, M. B., AND TAVERA, J. M., 1988, Magnetostratigraphy across the Berriasian-Valanginian stage boundary (Early Cretaceous) at Cehegín (Murcia Province, southern Spain): Earth and Planetary Science Letters, v. 87, p. 205–215.
- OGG, J. G., HASENYAGER, R. W., WIMBLEDON, W. A., CHANNELL, J. E. T., AND BRALOWER, T. J., 1991a, Magnetostratigraphy of the Jurassic-Cretaceous boundary interval, Tethyan and English faunal realms: Cretaceous Research, v. 12, p. 455–482.
- OGG, J. G. AND LOWRIE, W., 1986, Magnetostratigraphy of the Jurassic/Cretaceous boundary: Geology, v. 14, p. 547–550.
- OGG, J. G. AND STEINER, M. B., 1991, Early Triassic magnetic polarity time scale—Integration of magnetostratigraphy, ammonite zonation and sequence stratigraphy from stratotype sections (Canadian Arctic Archipelago): Earth and Planetary Science Letters, v. 107, p. 69–89.
- OGG, J. G., STEINER, M. B., OLORIZ, F., AND TAVERA, J. M., 1984, Jurassic magnetostratigraphy: 1. Kimmeridgian-Tithonian of Sierra Gorda and Carrabuey, southern Spain: Earth and Planetary Science Letters, v. 71, p. 147–162.
- OGG, J. G., WIECZOREK, J., HOFFMANN, M., AND STEINER, M. B., 1991b, Jurassic magnetostratigraphy: 4. Early Callovian through Middle Oxfordian of Krakow Uplands (Poland): Earth and Planetary Science Letters, v. 104, p. 289–303.
- ORBELL, G., 1983, Palynology of the British Rhaeto-Liassic: Bulletin of the Geological Survey of Great Britain, v. 44, p. 1–44.
- OTTONE, E. G. AND GARCIA, G. B., 1991, A Lower Triassic microspore assemblage from the Puesto Viejo Formation, Argentina: Reviews of Palaeobotany and Palynology, v. 68, p. 217–232.
- OWEN, H. G., 1984, Albian stage and substages boundaries: Bulletin of the Geological Society of Denmark, v. 33, p. 183–189.
- OWEN, H. G., 1988, The ammonite zonal sequence and ammonite taxonomy in the *Douvilleiceras mammillatum* Superzone (Lower Albian) in Europe: Bulletin of the British Museum of Natural History (Geology), v. 44, p. 177–231.
- PALMER, A. R., compiler, 1983, Decade of North American Geology (DNAG). Geologic Time Scale: Geology, v. 11, p. 503–504.
- PESSAGNO, E. A. AND BLOME, C. D., 1990, Implications of new Jurassic stratigraphic, geochronometric and paleolatitudinal data from the western Klamath terrane (Smith River and Rogue Valley substitute): Geology, v. 18, p. 665–668.
- PRINGLE, M. S., 1992, Radiometric ages of basaltic basement recovered at sites 800, 801 and 802, Leg 129, western Pacific Ocean: College Station, Proceedings of the Ocean Drilling Program, Scientific Results, v. 129, p. 389–404.
- PRINGLE, M. S., 1995, Radiometric dating of seamount edifices of guyots, western Pacific: Proceedings of the Ocean Drilling Program, Scientific Results, v. 144, in press.
- PRINGLE, M. S., OBRADOVICH, J. D., AND DUNCAN, R. A., 1992, Estimated age for magnetic anomaly M0 and Interval ISEA, and a minimum estimate for the duration of the Aptian: Eos, v. 73, p. 633.
- RAO, C. R., 1973, Linear Statistical Inference and Its Applications: New York, Wiley, 625 p.
- REINSCH, C. H., 1967, Smoothing by spline functions: Numerische Mathematik, v. 16, p. 451–454.
- RENNE, P. R. AND BASU, A. R., 1991, Rapid eruption of the Siberian Traps flood basalts at the Permo-Triassic boundary: Science, v. 253, p. 176–179.
- ROBASZYNSKI, F., AMÉDRO, F., (coord.), FOUCHER, J.-C., GASPARD, D., MAGNIEZ-JANNIN, F., MANIVIT, H., AND SORNAY, J., 1980, Synthèse biostratigraphique de l'Aptien au Santonien du Boulonnais. A partir de sept groupes paléontologique: Foraminifères, nannoplancton, dinoflagellés et macrofaunes. Zonations micropaléontologiques intégrées dans le cadre du Crétacé boréal nord-européen: Revue de Micropaléontologie, v. 22, p. 195–321.
- SALEEBY, J. B., 1984, Pb/U zircon ages from the Rogue River area, western Klamath belt, Klamath Mountains, Oregon: Geological Society of America, Abstracts with Programs, v. 16, p. 331.
- SCHUURMAN, W. M. N., 1979, Aspects of Late Triassic palynology. 3 Palynology of the latest Triassic and earliest Jurassic deposits of the Northern Limestone Alps in Austria and southern Germany, with special reference to a palynological characterization of the Rhaetian Stage in Europe: Reviews of Palaeobotany and Palynology, v. 27, p. 53–75.
- SHARPTON, V. L., DALRYMPLE, G. B., MARIN, L. E., RYDER, G., SCHURAYTZ, B. C., AND URUTIA-FUCUGAUCHI, J., 1992, New links between the Chicxulub impact structure and the Cretaceous/Tertiary boundary: Nature, v. 359, p. 819–821.
- SNELLING, N. J., ed., 1985, The Chronology of the Geological Record: Oxford, Blackwell Scientific Publishers, Geological Society of London Memoir 10, 343 p.
- STEINER, M. B., OGG, J. G., MELENDEZ, G., AND SEQUIEROS, L., 1986, Jurassic magnetostratigraphy: 2. Middle-Late Oxfordian of Aguilón, Iberian Cordillera, northern Spain: Earth and Planetary Science Letters, v. 76, p. 151–166.
- SWISHER, C. C., GRAJALES-NISHIMURA, J. M., MONTANARI, A., MARGOLIS, S. V., CLAEYES, P., ALVAREZ, W., RENNE, P., CEDILLO-PARDO, E., MUARASSEE, F., CURTIS, G. H., SMITH, J., AND McWILLIAMS, M. O., 1992, Coeval $^{40}\text{Ar}/^{39}\text{Ar}$ ages of 65.0 Million years ago from Chicxulub Crater melt rock and Cretaceous-Tertiary boundary tektites: Science, v. 257, p. 954–958.
- TAMAKI, K. AND LARSON, R. L., 1988, The Mesozoic tectonic history of the Magellan Microplate in the western Central Pacific: Journal of Geophysical Research, v. 93, p. 2857–2874.
- TAYLOR, J. R., 1982, An Introduction to Error Analysis: Mill Valley, University Science Books, 253 p.
- THORKELSON, D. J., MARSDEN, H., AND MORTENSEN, J., 1991, Early Jurassic volcanism north of the Bowser Basin and its role in paired subduction beneath Stikinia: Geological Society of America Abstracts and Programs, v. 23, 5, p. A191.
- THORKELSON, D. J., MORTENSEN, J. K., MARSDEN, H., AND TAYLOR, R. P., 1994, Age and tectonic setting of Early Jurassic episodic volcanism along the northeastern margin of the Hazelton Trough, northern British Columbia: Boulder, Geological Society of America, Special Paper, in press.
- THOMSON, R. C. AND SMITH, P. L., 1992, Pliensbachian (Lower Jurassic) biostratigraphy and ammonite fauna of the Spatsizi area, North-Central British Columbia: Bulletin of the Geological Survey of Canada, v. 437, p. 1–73.
- TOZER, E. T., 1967, A standard for Triassic time: Bulletin of the Geological Survey of Canada, v. 156, 103 p.
- VAN HINTE, J., 1976, A Jurassic time scale: American Association of Petroleum Geologists Bulletin, v. 60, p. 489–497.
- WARRINGTON, G., 1974, Studies in the palynological biostratigraphy of the British Trias. 1. Reference sections in West Lancashire and North Somerset: Reviews of Palaeobotany and Palynology, v. 17, p. 133–147.
- WEITSCHAT, W. AND DAGYS, A. S., 1989, Triassic biostratigraphy of Svalbard and a comparison with NE-Siberia: Mitteilungen aus dem Geologisch-Paläontologischen Institut der Universität Hamburg, v. 68, p. 179–213.
- WESTERMANN, G. E. G., 1984, Gauging the duration of stages: A new approach for the Jurassic: Episodes, v. 7, p. 26–28.
- WESTERMANN, G. E. G., 1988, Duration of Jurassic stages based on averaged and scaled subzones, in Agterberg, F. P. and Rao, C. N., eds., Recent Advances in Quantitative Stratigraphic Correlation: Dehli, Hindustan Publishing Company, p. 90–100.
- YIN H., 1993, A proposal for the global stratotype section and point (GSSP) of the Permian-Triassic boundary: Albertiana, v. 11, p. 4–30.
- ZAPFE, H., 1983, Das Forschungsprojekt "Trias of the Tethys Realm" (I.G.C.P. Project No. 4). Abschlussbericht, in Zapfe, H., ed., Neue Beiträge zur Biostratigraphie der Tethys Trias: Schriftenreihe der Erdwissenschaftlichen Kommissionen, Österreichisch Akademie Wissenschaft, v. 5, p. 7–16.

APPENDIX 1.—RADIOMETRIC DATA BASE FOR MESOZOIC STRATA

List of entire dataset and selected radiometric dates employed in the maximum likelihood estimates for Mesozoic stage boundaries. For further explanation see text.

Stages: The stage units heading groups of dates are approximate classification units, and bear no influence on the use of the maximum likelihood method used to calculate the age of stage boundaries. For the latter the age brackets (see above) are important. The stage bracket numbering largely corresponds to the coding used in PTS89.

Trial age: Initial estimate of stage boundary age for maximum likelihood calculations.

Number of zones: The number of (sub)zones is based on the highest-resolution ammonite zonal path.

Listing: Unique reference number for date; most items listed as new or revised are discussed in Appendix 2. Total number of dates = 323.

Date: Age date in Ma units.

Standard deviation (s): 1 standard deviation. Items listed as "revised" have had the standard deviation recalculated according to weighted averaging (Taylor, 1982) with the assumptions that the dates involved are from populations of radiometric dates with different standard deviations in the same or closely comparable samples, as listed in the cited literature. A "*" indicates an arbitrary standard deviation of 1 my (1σ). See explanations under "Brackets" and in text.

Brackets: This is the principal standardized tool to assign chronostratigraphic uncertainty to the relative age of sediments with a specific radiometric age date. The bracket refers to the relative age of sediments immediately above and below the dated level. The A (above) and B (below) coding of geologic stages follows the scheme of PTS89. A number "1" in column C marks a directly estimated age for a stage boundary (see text); these items include numerically interpolated ages for late Cretaceous stage boundaries, and magnetostratigraphic interpolated ages for late Jurassic to early Cretaceous stage boundaries using the Hawaiian marine magnetic anomaly sequence, and radiometric age estimates in Pliensbachian, Hettangian, and at the Anisian/Ladinian and Permian/Triassic boundaries.

Method: "1" = high-temperature; "2" = low-temperature minerals; KAr WR or KAr Bi indicate ages from bentonites coded as high-temperature.

Comments: Reference or source of age data and brief annotation. The majority of items are taken from Table 4.2 in PTS89, cited according to this table, and from the smaller Appendix B in EX88, also cited accordingly. "Revised" means that the data quoted by these authors has been re-interpreted using standard averaging procedures of analytical data, as documented in Appendix 2. "New" means that the item was not listed previously in Table 4.2 in PTS89, Appendix B in EX88, or NDS82.

Stage (Bracket); Number of Zones

Brackets

Listing	Date	Standard Deviation	A	B	C	Method	Comments
<i>Thanetian (bracket 18)</i>							
1	52.60	1.20	18	18	2	NDS27	
2	53.10	1.65	18	18	2	NDS17	
3	53.50	1.90	18	18	1	B/MH ArAr WR	
4	54.10	1.00	18	18	2	NDS28	
5	54.40	0.97	18	18	2	NDS38	
6	54.80	1.75	18	18	2	NDS16a	
7	55.10	0.20	18	18	1	new; CK92	
8	56.00	0.95	18	18	2	NDS39	
9	56.60	3.40	18	18	2	NDS22	

Stage (Bracket); Number of Zones continued

Listing	Date	Standard Deviation	Brackets			Method	Comments
			A	B	C		
10	57.50	0.67	18	18	2	NDS113	
11	57.50	1.50	18	18	2	NDS16b	
12	58.25	0.31	18	18	2	FIT77	
13	58.87	2.01	18	18	2	PTS105	
14	59.90	2.53	18	18	2	PTS113	
15	60.92	3.00	18	18	2	PTS106	
16	61.02	0.45	18	18	2	FHMB1	
17	59.44	0.70	18	19	2	NDS55	
18	60.50	0.35	18	19	2	NDS247	
<i>Danian (bracket 19)</i>							
19	60.10	1.82	1	19	1	PTS306 KAr WR	
20	61.25	1.08	19	19	2	NDS92	
21	62.06	1.50	19	19	1	PTS362 KAr BiSd	
22	62.10	1.55	19	19	2	NDS114	
23	63.00	0.32	19	19	1	NDS126a KAr Sd	
24	63.03	0.63	19	19	2	NDS120	
25	63.70	0.32	19	19	1	NDS127a	
26	63.90	0.35	19	19	1	NDS127b UPb Zr	
27	65.40	1.10	19	19	2	BLM	
28	65.50	1.00	19	19	1	OSK ArAr Sd	
29	65.80	0.70	19	19	2	NDS103	
30	65.80	0.80	19	19	2	OB2	
31	66.00	0.90	19	20	1	OB1 ArAr Sd	
32	66.34	2.41	19	19	2	PTS307 KAr Fl	
33	67.14	3.02	19	19	1	PTS329 KAr WR	
34	65.00	0.04	19	20	1	new; see text	
<i>Maastrichtian (bracket 20); trial age 65.0 Ma number of zones = 15 (approx)</i>							
35	67.17	5.00	16	20	2	PTS198a	
36	65.41	1.00	20	20	2	PTS364 KAr Fl	
37	66.70	1.00	20	20	2	NDS36	
38	66.80	2.00	20	20	1	S3 KAr WR	
39	66.80	0.55	20	20	1	new; ArAr Sd; OB93	
40	67.00	0.70	20	20	1	PTS365 KAr BiSd	
41	67.05	3.02	20	20	2	A449	
42	69.00	0.70	20	20	2	NDS104	
43	69.80	2.10	20	20	1	S8	
44	69.80	2.10	20	20	1	S7 KAr WR	
45	69.42	0.18	20	20	1	new; ArAr Sd; OB93	
46	70.40	2.11	20	20	2	S6	
47	70.63	1.93	20	20	2	PTSS4	
48	71.50	0.74	20	20	2	NDS139	
49	69.50	2.10	20	21	1	S9	
50	70.30	2.11	20	21	2	S4	
51	74.18	0.77	20	21	2	PTS365 KAr BiSd	
52	71.60	0.70	20	21	1	new; McArthur and others (1993)	
53	71.30	0.25	20	21	1	new; OB93	
<i>Campanian (bracket 21); trial age 71.3 Ma; number of zones = 23</i>							
54	71.60	1.35	21	21	2	NDS116	
55	72.98	0.70	21	21	2	NDS105 KAr Fl	
56	73.19	0.70	21	21	2	NDS105; McArthur and others (1993)	
57	73.40	1.00	21	21	1	OSK ArAr Sd	
58	73.35	0.17	21	21	1	new; ArAr Sd; OB93	
59	73.90	0.70	21	21	2	NDS105	
60	74.00	2.22	21	21	1	S5 KAr WR	
61	74.31	0.70	21	21	2	NDS105	
62	74.52	0.70	21	21	2	NDS105	
63	74.60	1.35	21	21	2	NDS116	
64	75.33	0.66	21	21	2	NDS140	
65	75.37	0.18	21	21	1	new; ArAr Sd; OB93	
66	75.89	0.36	21	21	1	new; ArAr Sd; OB93	
67	75.50	0.60	21	21	1	AB ArAr Sd	
68	75.20	0.50	21	21	1	new; CK92	
69	79.12	0.80	21	21	2	NDS106	
70	79.30	0.67	21	21	2	NDS117	
71	79.73	0.80	21	21	2	NDS106	
72	79.83	2.00	21	21	1	A410	
73	80.04	0.80	21	21	2	NDS106	

Stage (Bracket); Number of Zones continued

Listing	Date	Standard Deviation	Brackets			Method	Comments
			A	B	C		
74	80.54	0.55	21	21		1	new; Ar/Ar Sd; OB93
75	81.50	1.50	21	21		1	NDS163 KAr WR
76	81.71	0.17	21	21		1	new; Ar/Ar Sd; OB93
77	81.88	3.00	21	21		1	A508 KAr SdBi
78	82.90	2.84	21	21		2	PTS62
79	84.02	5.00	21	21		2	A417
80	83.50	0.25	21	22	1	1	new; OB93
<i>Santonian (bracket 22); trial age 83.5 Ma; number of zones = 5</i>							
81	82.38	1.50	22	22		1	HMFT Rb/Sr WRB _i
82	83.91	0.21	22	22		1	new; Ar/Ar Sd; OB93
83	84.09	0.20	22	22		1	new; Ar/Ar Sd; OB93
84	84.90	0.15	22	22		1	new; Ar/Ar Sd; OB93
85	84.40	1.00	22	22		1	OSK Ar/Ar Sd
86	84.43	0.80	22	22		2	NDS107
87	84.94	2.99	22	22		2	PTS229
88	89.03	3.00	22	22		1	A509 KAr Sd
89	86.30	0.25	22	23	1	1	new; OB93
<i>Coniacian (bracket 23); trial age 86.3 Ma; number of zones = 4</i>							
90	85.87	0.89	23	23		2	NDS83a
91	86.00	4.00	23	23		1	MB Ar/Ar WR
92	86.80	1.65	23	23		2	NDS86
93	86.92	0.20	23	23		1	new; Ar/Ar Sd; OB93
94	87.02	0.65	23	23		2	NDS83b
95	88.34	0.30	23	23		1	new; Ar/Ar Sd; OB93
96	88.67	3.07	23	23		2	PTS57
97	90.50	1.05	23	23		2	NDS60
98	88.82	0.90	23	24		2	NDS108
99	88.70	0.25	23	24	1	1	new; OB93
<i>Turonian (bracket 24); trial age 88.7 Ma; number of zones = 13</i>							
100	92.20	2.00	1	24		1	LAN1 Ar/Ar Hb
101	87.30	2.05	24	24		2	NDS94b
102	87.60	1.30	24	24		2	NDS82b
103	88.10	0.75	24	24		2	NDS227
104	88.17	1.50	24	24		2	NDS82a
105	88.70	1.10	24	24		2	NDS164
106	89.50	0.75	24	24		2	NDS226a
107	90.10	3.60	24	24		1	SM1
108	90.21	0.36	24	24		1	new; Ar/Ar Sd; OB93
109	90.51	0.22	24	24		1	new; Ar/Ar Sd; OB93
110	90.97	0.90	24	24		2	NDS109
111	93.69	2.40	24	24		2	SM2
112	88.75	1.26	24	25		2	NDS95
113	92.09	3.00	24	25		1	A510 KAr Sd
114	92.76	0.43	24	25		2	NDS118
115	93.25	0.28	24	24		1	new; Ar/Ar Sd; OB93
116	93.40	0.31	24	24		1	new; Ar/Ar Sd; OB93
117	93.30	0.10	24	25	1	1	new; OB93
<i>Cenomanian (bracket 25); trial age 93.3 Ma; number of zones = 23 (approx)</i>							
118	91.83	3.67	1	25		1	PTS335 KAr WR
119	87.60	1.60	25	25		2	NDS69
120	87.93	4.00	25	25		2	A418
121	89.50	1.65	25	25		2	NDS81
122	89.80	1.80	25	25		2	NDS59
123	90.50	3.00	25	25		2	NDS62
124	90.60	0.75	25	25		2	NDS226b
125	90.86	3.63	25	25		2	PTS209
126	91.20	0.73	25	25		2	NDS81
127	92.20	1.55	25	25		2	NDS85
128	92.40	0.82	25	25		2	NDS119a
129	93.30	0.78	25	25		2	NDS80a
130	93.42	0.90	25	25		2	NDS110
131	93.51	0.14	25	25		1	new; Ar/Ar Sd; OB93
132	93.90	0.36	25	25		1	new; Ar/Ar Sd; OB93
133	93.49	0.45	25	25		1	new; Ar/Ar Sd; OB93
134	94.20	0.35	25	25		2	NDS211
135	94.24	0.90	25	25		2	NDS110
136	94.63	0.30	25	25		1	new; Ar/Ar Sd; OB93
137	94.70	0.55	25	25		2	NDS62
138	94.93	0.27	25	25		1	new; Ar/Ar Sd; OB93

Stage (Bracket); Number of Zones continued

Listing	Date	Standard Deviation	Brackets			Method	Comments	
			A	B	C			
139	95.00	1.00	25	25		2	NDS64	
140	95.00	1.00	25	25		2	NDS96	
141	95.32	0.66	25	25		2	NDS80b	
142	95.40	0.75	25	25		2	NDS67	
143	95.78	0.30	25	25		1	new; Ar/Ar Sd; OB93	
144	95.86	0.22	25	25		1	new; Ar/Ar Sd; OB93	
145	96.53	1.07	25	25		2	NDS119b	
146	97.40	1.25	25	25		2	NDS68	
147	97.69	3.91	25	25		2	PTS211	
148	97.17	0.34	25	25		1	new; Ar/Ar Sd; OB93	
149	98.22	3.04	25	25		2	PTS226	
150	98.52	0.20	25	25		1	new; Ar/Ar Sd; OB93	
151	98.54	0.35	25	25		1	new; Ar/Ar Sd; OB93	
152	98.74	0.30	25	25		1	new; Ar/Ar Sd; OB93	
153	96.50	0.60	25	128		1	TWH1 UPb Zr	
154	102.31	3.00	25	26		1	PTS202 KAr BiSd	
155	95.00	1.00	25	26		2	revised; NDS96	
156	98.50	0.25	25	26	1	1	new; OB93	
<i>Albian (bracket 26); trial age 98.5 Ma; number of zones = 25</i>								
157	113.85	2.00	20	26		1	PTS217 UPb Zr	
158	96.18	3.11	26	26		2	PTS230	
159	96.18	3.14	26	26		2	PTS51	
160	96.50	1.35	26	26		2	NDS145	
161	97.50	1.00	26	26		2	NDS111	
162	97.60	0.48	26	26		2	NDS144b	
163	97.60	1.00	26	26		1	NDS111 KAr Sd	
164	98.22	2.00	26	26		1	PTS204 KAr BiSd	
165	98.22	3.22	26	26		2	PTS56	
166	98.35	1.16	26	26		2	NDS65	
167	98.70	2.50	26	26		2	NDS61	
168	98.90	1.23	26	26		2	NDS97a	
169	99.00	1.12	26	26		2	NDS63	
170	99.24	3.38	26	26		2	PTS228	
171	99.25	1.39	26	26		2	NDS66	
172	99.50	1.55	26	26		2	new; KAr; Odin and Hunziker (cited in OB93)	
173	98.40	1.60	26	26		2	new; KAr; Odin and Hunziker (cited in OB93)	
174	99.40	0.65	26	26		2	NDS157a	
175	99.60	2.50	26	26		2	NDS67	
176	99.70	1.10	26	26		2	NDS144d	
177	99.72	0.76	26	26		2	NDS79b	
178	99.77	0.98	26	26		2	NDS78a	
179	100.00	0.80	26	26		2	NDS144a	
180	100.27	3.00	26	26		2	PTS242	
181	100.60	0.50	26	26		2	NDS144c	
182	100.60	2.50	26	26		2	NDS97	
183	100.62	4.02	26	26		2	PTS212	
184	100.62	4.00	26	26		2	PTS220	
185	102.57	4.10	26	26		1	PTS336 KAr WR	
186	103.10	0.95	26	26		2	NDS144e	
187	103.55	4.00	26	26		2	A428	
188	103.58	0.72	26	26		2	NDS70	
189	104.40	1.05	26	26		2	NDS157b	
190	105.36	0.91	26	26		2	NDS78b	
191	106.00	0.50	26	26		2	NDS143	
192	107.10	0.15	26	26		2	A429	
193	110.48	3.87	26	26		2	new; OB93	
194	114.76	4.01	26	26		2	PTS219	
195	116.05	1.24	26	26		2	PTS223	
196	104.53	3.89	26	27		2	NDS98a	
197	111.00	2.00	26	27		1	new; Marcoux and others (1987)	
198	112.00	0.50	26	27	1	1	new; OB93	
<i>Aptian (bracket 27); trial age 112 Ma; number of zones = 9</i>								
199	105.80	1.31	27	27		2	NDS77a	
200	107.30	1.95	27	27		2	NDS71	
201	108.20	0.95	27	27		2	NDS146	
202	109.30	3.00	27	27		2	NDS188 KAr Fl	

Stage (Bracket); Number of Zones continued

Listing	Date	Standard Deviation	Brackets			Method	Comments
			A	B	C		
203	112.05	1.17	27	27		2	NDS98b
204	113.00	1.00	27	27		1	JE1 ArAr Sd
205	113.00	0.70	27	27		1	OSK ArAr Sd
206	114.00	0.65	27	27		1	new; ArAr Sd; OB93
207	115.00	0.03	27	27		1	new; Pringle and others (1992)
208	115.47	1.26	27	27		2	NDS77b; revised PTS89
209	117.62	3.88	27	27		2	PTS50
210	125.26	6.00	27	28		1	SMYH1
211	124.00	1.00	27	28		1	new; Ar/Ar; Herbert (1992)
212	121.00	0.50*	27	28		1	1 new; OB93 and this study
<i>Barremian (bracket 28); trial age 122 Ma; number of zones = 9</i>							
213	123.50	0.50	28	28		1	new; Pringle (pers. commun., 1993, see text)
214	132.83	5.31	28	30		2	PTS215
215	126.00	1.50	28	29		2	NDS162b
216	126.90	1.00*	28	29	1	1	new; this study
<i>Hauterivian (bracket 29); trial age 127 Ma; number of zones = 12</i>							
217	133.50	2.84	1	29		1	LBM1
218	119.30	0.45	29	29		2	NDS162a
219	133.60	2.00	29	33		1	PTS75R KAr BiHb
220	127.60	0.20	29	29		1	new; Pringle (pers. commun., 1993, see text)
221	136.00	2.00	29	33		1	LJ3
222	132.00	1.00*	29	30	1	1	new; this study
<i>Valanginian (bracket 30); trial age 130 Ma; number of zones = 10</i>							
223	126.81	3.80	1	30		1	A406
224	122.09	4.88	30	30		2	PTS322
225	125.02	5.00	30	30		2	A430
226	136.50	2.70	30	30		1	LJ4 KAr Bi
227	146.00	4.26	30	31		1	LBM2
228	138.40	1.00*	30	31	1	1	new; this study
<i>Berriasian (bracket 31); trial age 135 Ma; number of zones = 7</i>							
229	130.88	5.24	1	31		1	PTS238 KAr Bi
230	133.95	4.00	31	31		2	PTS177
231	138.00	4.00	31	32		2	W misc
232	137.10	0.60	31	31		1	new; Bralower and others (1990)
233	144.20	1.00*	31	32	1	1	new; this study
<i>Tithonian (bracket 32); trial age 142 Ma; number of zones = 20</i>							
234	131.10	1.50	32	32		2	revised EX88; NDS76
235	132.83	5.31	32	32		2	PTS322
236	134.97	4.00	32	32		2	PTS178
237	135.53	1.20	32	32		2	revised EX88, PTS89; NDS99
238	141.40	1.75	32	32		2	NDS228
239	152.50	2.00	32	128		1	HMP2 UPb Zr
240	154.00	2.00	32	128		1	HMP3 UPb Zr
241	158.42	3.57	32	128		1	H445 KAr Hb
242	150.70	1.50*	32	33	1	1	new; this study
243	139.66	4.00	29	32		1	PTS76
<i>Kimmeridgian (bracket 33); trial age 147 ma; number of zones = 15</i>							
244	150.50	2.00	1	33		1	HS1 UPb Zr
245	155.00	3.00	33	34		1	revised; SCH1; UPb Zr
246	153.32	4.60	1	33		2	A480
247	155.00	3.00	1	33		1	SBG UPb Zr
248	155.28	4.66	1	33		1	A481
249	138.45	1.06	33	33		2	revised EX88; NDS142
250	153.50	2.00*	33	34	1	1	new; this study
<i>Oxfordian (bracket 34); trial age 154 Ma; number of zones = 20</i>							
251	155.30	3.40	34	34		1	new; Ludden (1992)
252	148.00	0.87	34	34		2	revised EX88; NDS141 (KAr)
253	157.00	2.00	34	128		1	HS2 UPb Zr
254	161.00	2.00	34	128		1	HMP1 UPb Zr
255	162.00	2.00	34	128		1	HMP4 UPb Zr

Stage (Bracket); Number of Zones continued

Listing	Date	Standard Deviation	Brackets			Method	Comments
			A	B	C		
256	160.00	2.00*	34	34		1	new; this study
<i>Callovian (bracket 35); trial age 159 Ma; number of zones = 18</i>							
257	159.00	5.00	32	35		1	revised PTS89; BL1 KAr Hb
258	166.80	4.50	35	35		1	new; Pringle (1992)
<i>Bathonian (bracket 36); trial age 164 Ma; number of zones = 15</i>							
259	160.14	6.00	36	37		1	A419 KAr WR
260	168.50	4.00	36	37		1	BFSB6R KAr WR
261	173.00	4.00	27	37		2	WEST2 KAr Fl
262	168.92	2.00	32	37		2	PTS90
263	161.30	3.20	35	37		1	new; Odin (1992, Bull 9)
<i>Bajocian (bracket 37); trial age 169 Ma; number of zones = 20</i>							
264	168.00	2.00	37	37		1	new; KAr, WHR; Gillot in Odin (1992b)
265	172.00	2.00	37	37		1	new; KAr, WHR; Gillot in Odin (1992b)
266	171.00	3.50	37	37		1	NDS182 KAr Hb
<i>Aalenian (bracket 38); trial age 176 Ma; number of zones = 9</i>							
267	171.67	5.15	34	38		2	A479
<i>Toarcian (bracket 39); trial age 179 Ma; number of zones = 24</i>							
268	182.50	2.84	39	40		1	NDS183a KAr Hb
269	185.00	3.00	39	40		1	HLB1 ArAr BiFl
270	190.00	7.00	39	40		1	NDS183b RbSr Hb
271	198.86	2.65	39	40		1	NDS184R KAr BiHb
272	197.60	2.50	39	41		1	NDS184R ArAr Bi
273	191.25	3.38	39	45		1	FW40 KAr WRFI
274	193.00	1.50	39	45		1	FW42 KAr WR
275	193.00	1.50	39	45		1	FW41 RbSr WR
<i>Pliensbachian (bracket 40); trial age 188 Ma; number of zones = 15</i>							
276	194.12	0.62	40	40	1	1	new; Thorkelsen and others (1994)
<i>Sinemurian (bracket 41); trial age 197 Ma; number of zones = 17</i>							
277	203.20	1.95	1	41		1	revised; NDS181 KAr Hb
278	196.00	4.50	40	43		1	revised; Forster and Warrington (1985)
279	195.00	4.20	40	43		1	revised; Forster and Warrington (1985)
<i>Rhaetian (bracket 43); trial age 205 Ma; number of zones = 6</i>							
280	200.00	5.00	41	42		1	NDS203 KAr WR
281	202.40	2.13	41	42		2	NDS248
282	206.00	6.00	41	43		2	WEST1 KAr Fl
<i>Hettangian (bracket 42); trial age 201 Ma; Number of zones = 8</i>							
283	210.36	6.00	1	42		1	A478 KAr Hb
284	205.00	2.50	42	44		2	NDS177
285	201.00	0.70	42	42	1	1	new; Hodych and Dunnig (1992)
286	201.10	0.71	42	42	1	1	" "
287	216.00	2.00	43	44		1	NDS137a (T13 in EX88) KAr BiHb
288	216.00	3.00	43	44		1	NDS137b RbSr WRBi
289	213.00	3.50	43	128		1	NDS199 KAr WR
<i>Norian (bracket 44); trial age 210 Ma; number of zones = 16</i>							
290	204.00	4.50	1	44		1	NDS174 KAr WR
291	207.00	1.03	1	44		1	FW36 RbSr WR
292	207.00	4.00	1	44		1	NDS178b
293	208.00	2.00	1	44		1	NDS179 KAr Hb
294	210.00	1.05	1	44		2	NDS204
295	210.00	4.00	1	44		1	NDS178a KAr HbBi
296	215.70	2.70	1	44		1	NDS178R ArAr HbBi
297	211.00	4.22	44	44		1	KM1 UPb Zr
298	221.00	6.00	44	45		1	NDS170 KAr Hb
<i>Carnian (bracket 45); trial age 220 Ma; number of zones = 10</i>							
299	215.82	5.00	1	45		1	PTS160 UPb Ur
300	220.00	5.00	1	45		1	NDS171 KAr HbBi
301	231.00	2.48	1	45		1	NDS201a KAr Ph
302	229.00	2.50	45	45		1	NDS187 KAr WR
303	230.50	2.48	45	46		1	NDS193 KAr WR
<i>Ladinian (bracket 46); trial age 230 Ma; number of zones = 12</i>							
304	225.00	2.00	1	46		2	FW33

Stage (Bracket); Number of Zones continued

Listing	Date	Standard Deviation	Brackets			Method	Comments
			A	B	C		
305	225.68	8.00	1	46		1	PTS358b
306	233.50	2.48	1	46		2	NDS194
307	235.78	7.07	1	46		1	PTS361
308	237.06	3.00	1	46		1	PTS361
309	233.00	4.50	46	47	1	1	NDS196
310	232.00	4.50	46	47	1	1	"
<i>Anisian (bracket 47); trial age 235 Ma; number of zones = 16</i>							
311	237.00	2.20	47	49		1	NDS186; revised
312	240.00	4.80	47	47		1	KM2
313	243.00	2.12	47	128		1	NDS194
<i>Olenekian and Induan (bracket 48); trial age 240 Ma; number of zones: Olenekian-8, Induan-9</i>							
314	248.00	7.00	48	49		1	NDS158
315	243.92	7.32	48	49		1	PTS357
316	250.00	4.94	48	84		2	PTS346
317	248.30	0.30	48	49	1	1	new; ArAr, WHR; Renne and Basu (1991)
318	247.50	0.70	48	49	1	1	new; ArAr, WHR; Renne and Basu (1991)
<i>Tatarian (bracket 49); trial age 248 Ma</i>							
319	251.20	1.70	48	49		1	new; ArAr, Zr; Clauque-Long and others (1992)
320	250.00	3.00	48	49		1	new; RbSr, Sd; Odin (1992b)
321	248.85	8.71	49	49		1	A434; KAr, WR
322	250.00	1.79	49	49		1	NDS205; KAr, WR
323	253.00	2.50	49	49		1	FW22; KAr, WR

APPENDIX 2.—COMMENTS ON AGES IN DATABASE

Comments on selected radiometric and chronostratigraphic items, listed in Appendix 1 as "new" or "revised."

Items 39, 45, 58, 65, 66, 68, 76, 82, 83, 84, 93, 95, 108, 109, 115, 116, 131, 132, 133, 136, 138, 143, 144, 148, 150, 151, 152, 172, 173, 192, 206, 211, 232. These items are Ar/Ar dates on sanidine in bentonites as listed in OB93 and have been normalized to an age of 520.4 Ma for the lab calibration standard MMhb-1.

Item 155: NDS96 (95.00 ± 1.00 Ma). PTS89 assigns the relative age as intra Albian. The original designation in NDS82 is late Albian to early Cenomanian Age; hence, we recode 26–26 as 25–26.

Item 203: NDS98b (112.05 ± 1.17 Ma). EX88 (item C26) quote an age of 112.0 ± 3.3 Ma (2σ). The actual dates are 111.7 ± 1.75 Ma (1σ) and 112.4 ± 1.75 Ma (1σ), which averages as 112.05 ± 1.17 Ma. The latter date is also used in PTS89.

Item 208: NDS77 (115.47 ± 1.26 Ma). PTS89 cite an age of 115.80 ± 1.24 Ma for the average of two Rb/Sr ages on Late Aptian glauconites. Our averaging procedure yields 115.47 ± 1.26 Ma.

Item 211: (124.00 ± 1.00 Ma). Herbert (1992) quotes an average Ar/Ar age of 124.00 ± 1.00 Ma on reversed magnetized plutons from Canada (Foland and others, 1986), which may fit at the top of the M-reversal sequence. According to Foland and others (1986) paleo-inclination studies and the constant reversed polarity of the extensive pluton complex are indicative of emplacement within 2 my and certainly less than 5 my. Hence, the plutons may belong in one of the longer reversal sequences at the top of the M-sequence, and M3r is a good

candidate. This suggests the relative age for the plutons may be Barremian stage.

Item 213: (123.5 ± 0.5 Ma). Pringle (pers. commun., 1993) reports 123.5 ± 0.5 Ma (1σ) for polarity chron M1r on MIT seamount (Ar/Ar on oceanic basement lavas). The relative age is latest Barremian.

Items 215, 218: NDS162a,b. PTS89 twice use the same age of 126.0 ± 1.5 Ma, listed as NDS162b, once for Hauterivian strata and once for Barremian strata. The glauconites are from a level at about the Hauterivian-Barremian boundary, hence we assign a Hauterivian-Barremian age. EX88 does not utilize this age, but only NDS162a of 119.3 ± 0.45 Ma for latest Hauterivian glauconites. NDS82 mentions that this second and younger age might be unreliable due to upwarping of the adjacent salt diaper. However, NDS162b also maybe unreliable due to mineral "inclusions."

Item 220: (127.6 ± 0.2 Ma). Using Ar/Ar dating of basement basalts of Resolution Guyot (ODP Site 866A), Pringle (pers. commun., 1993) dates polarity chron M5r of ?late Hauterivian age, as 127.6 ± 0.2 Ma (1σ).

Item 243: (139.66 ± 4.0 Ma). PTS89 reference PTS #76 is cited as Kimmeridgian age, at location Loomis, Sierra Nevada, California. The original age is given as 143 Ma but based on a different noralization. These quartz-diorite or gabbro intrusions are associated with the "Nevadan orogeny" and intrude the Mariposa Formation, which is dated by ammonites as Late Oxfordian-Early Kimmeridgian Age. The upper age is less certain, but is definitely pre-Barremian, because related batholiths (e.g., Shasta Bally) are overlain by sediments of this age. There is inadequate control on the age of the intrusions, with a possible Kimmeridgian through Hauterivian range.

Item 251: (155.30 ± 3.40 Ma). M26r (Late Oxfordian) age ocean crust at ODP Site 765, Argo Abyssal Plain, is dated at 155.3 ± 3.4 Ma, using the Ar/Ar method (Ludden, 1992).

Item 257: Callovian-Tithonian interval. PTS89 quotes a K/Ar age of 159 Ma for intra Callovian volcanics, dated by ammonites in the Coloradoito Formation of California (Boles and Landis, 1984). This age is revised to involve volcanics underlain by Callovian strata and overlain by Tithonian radiolarites, hence the bracket changes from 35–35 to 32–35.

Item 258: Callovian Stage. Pringle (1992) dates oceanic crust at ODP Site 801 at 166.8 ± 4.5 Ma; sediment in the upper crust contain radiolarians of early Callovian or latest Bathonian Age. The crust slightly predates M38.

Item 263: brackets 35/37; "Bathonian" age. High-temperature radiometrics of 161.3 ± 3.2 Ma, on lavas associated with sediments younger than Bajocian Age, and older than Callovian sediments in the Caucasus (Odin, 1992b).

Items 264 and 265: Bajocian Stage. Gillot in Odin (1992b) dated volcanic hornblende with K/Ar as $168-172 \pm 2.0$ Ma. The rocks are identified as of Bajocian Age.

Item 276: Early Pliensbachian Stage. Thorkelsen and others (1994), and J. Mortensen (pers. commun., 1993) report three U/Pb ages of 194.8 ± 1.0 Ma, 193.7 ± 1.4 Ma, and 193.7 ± 0.95 Ma (1σ) on zircons in the Cold Fish volcanics, British Columbia. Ammonites in sedimentary beds alternating with the volcanics, include *Miltoceras* sp., *Tropidoceras* sp., *Metaderoceras* sp. aff. *talkeetnaense*, *Acanthopleuroceras* sp. aff. *A. stahli*, and *Metaderoceras evolutum*, and assign the Cold Fish

volcanics an early to middle Carixian (Early Pliensbachian) Age (Thomson and Smith, 1992).

Item 277: NDS181; earliest Jurassic Period. EX88 item J2 quote 204 ± 5.0 Ma for item NDS181 of Sinemurian-Early Pliensbachian relative age. The same item is quoted in PTS89 as 203 ± 1.95 Ma between Sinemurian and Recent. In fact, NDS181 quotes two ages: one at 204 ± 5 Ma and one 202 ± 6 Ma (2σ). PTS89 pooled these two dates and divided the combined standard deviation by the square root of the number of analysis. However, this is only correct if the standard deviation for both analysis are equal. The correctly interpolated age is 203.2 ± 1.95 Ma (1σ).

Item 280: NDS203. EX88 item J3 is NDS203. EX88 picks one value (202 ± 6 Ma) from NDS203 where in fact there are 2 age dates: 202 ± 6 Ma and 206 ± 6 Ma. The correct (pooled) age is 204 ± 4.24 Ma, used in this study. PTS89 gives an age for item NDS203 of 200 ± 5 Ma.

Item 311: NDS186. Brackets Anis/Induan interval: 237 ± 2.2 Ma (1σ) in tuffs; K/Ar high-temperature volcanic/sedimentary Puesto Viejo Formation in Argentina (NDS 186; item 28 in Forster and Warrington, 1985). The basal part of the formation has a palynological date, suggesting an Early Triassic Age (Induan, ?Olenekian; Ottone and Garcia, 1991).